A missing link between ancient and active mafic-hosted seafloor hydrothermal systems - Magmatic volatile influx in the exceptionally preserved Mala VMS deposit, Troodos, Cyprus

Andrew J. Martin[1,2], Iain McDonald[1], Gawen R.T. Jenkin[3], Katie A. McFall[1], Adrian J. Boyce[4], John W. Jamieson[2] and Christopher J. MacLeod[1]

[1] School of Earth and Ocean Sciences, Cardiff University, Cardiff, CF10 3AT, UK

[2] Department of Earth Sciences, Memorial University of Newfoundland, NL, Canada

[3] School of Geography, Geology and the Environment, University of Leicester, Leicester, LE1 7RH, UK

[4] Scottish Universities Environmental Research Centre, East Kilbride, G75 0QF, UK

Abstract

Reconciling observations between ancient volcanogenic massive sulfide (VMS) and actively forming seafloor massive sulfide (SMS) deposits is critical for understanding the sources and processes that govern metal enrichment in marine hydrothermal systems. For a mafic VMS deposit, the Mala VMS mound located within the Troodos ophiolite, Cyprus, is unusual as pyrite is enriched in magmatic volatile elements (Au, Cu, Te and Se), sulfide $\delta^{34}S$ values average -3.8‰ ± 1.9‰ (1σ, n=28), and gypsum averages +14.5‰ ± 2.0‰ (1σ, n=26) - in stark contrast to the bulk of Troodos VMS pyrite, which averages +4.6‰ ± 2.8‰. To date, this combination of features has only been observed in actively forming SMS deposits in immature, subduction-influenced environments and rarely in ancient VMS deposits hosted in felsic environments. Traditionally, the leaching of igneous rocks is considered as the primary source of metals in mafic VMS deposits. However, at Mala, and perhaps other active SMS deposits in mafic environments, we suggest that Au, Cu, Te and Se were *initially* sourced from the direct contribution of a magmatic volatile phase where SO_2 underwent disproportionation, a signature that is later overprinted by reacted seawater during deposit maturation and is therefore not usually preserved in ancient analogues. Thus, the exceptional preservation of Mala provides evidence of a magmatic volatile contribution in the early stages of mafic VMS deposit formation.

1. Introduction

Active SMS deposits form in a wide range of tectonic settings from mid-ocean ridges (Humphris et al., 1995) to island arcs (de Ronde et al., 2011) and back-arc basins (Herzig et al., 1998a). Differences in metal enrichment among tectonic environments are recognised and are thought to relate to variations in both source rock metal content and magmatic volatile flux into the hydrothermal system; however, the relative contribution of metal from these two sources remains poorly constrained and actively debated (Hedenquist and Lowenstern, 1994; Large, 1992; Moss et al., 2001; Ohmoto, 1996; Patten et al., 2020; Stanton, 1984; Yang and Scott, 1996). Linking processes between ancient and active seafloor hydrothermal systems is key to understanding factors that control metal enrichment in ancient VMS deposits, how this varies with VMS deposit maturation, and how this signature is preserved in ancient on-land analogues - a tool that can be utilised in mineral exploration to assess the potential metal endowment of VMS deposits.

A magmatic volatile phase in a hydrothermal system can potentially be a metal source, especially for metals such as Au, Cu, Te and Se (de Ronde et al., 2005; Keith et al., 2016a,2018a; Wohlgemuth-Ueberwasser et al., 2015; Yang and Scott, 1996; 2002). Gold adds value to a deposit and can be critical in making it economic, while Te and Se are increasingly of interest because of their use in solar electricity generation, and for the fact they may represent potential environmental contaminants (He et al., 2018; Keith et al., 2018b; Moss et al., 2013). Enrichment in these metals relates to the volatile-rich nature of melts generated in subduction-influenced environments (i.e. arcs and back-arc basins) and their ability to exsolve a volatile phase rich in Au, Cu, Te and Se providing an additional source of these metals to the overlying hydrothermal system (e.g., Hedenquist and Lowenstern, 1994; Williams-Jones and Heinrich, 2005; Yang and Scott, 1996). An enrichment in Au, Cu, Te and Se in active subduction-influenced hydrothermal fields is observed (Fuchs et al., 2019; Keith et al., 2016a; Wohlgemuth-Ueberwasser et al., 2015) but evidence in ancient VMS deposits is much more limited, especially away from volatile-rich subduction related environments, and in mafic VMS deposits in particular (Keith et al., 2016b; Martin et al., 2019, 2020). The ability to identify if this process operated in ancient hydrothermal ore-forming systems, especially mafic VMS systems that are typically considered as volatile-poor (Hannington et al.,

2005), would give greater confidence in predicting metal endowment and enrichment processes in active and ancient VMS deposits.

Previous studies focused on ancient VMS deposits have suggested that the addition of a magmatic volatile phase may provide an important source of metals (e.g., Huston et al., 2011; Large, 1992); moreover, studies indicate that magmatic volatile influx decreases or changes over time in response to developing fluid flow regimes below the seafloor (Large, 1992). This variation is subsequently preserved as systematic variations in trace metal geochemistry that vary with VMS deposit maturity, most notably for volatile trace metals such as Te and Se that are enriched in immature deposits (Huston et al., 1995; Large, 1992; Martin et al., 2020; Rouxel et al., 2004). In hydrothermal systems that are long-lived, trace metals are remobilized and redistributed and the initial magmatic volatile signature is overprinted by later fluid flow during zone refining within the VMS mound (Goldfard et al., 1983). We hypothesise that the magmatic volatile signature in ancient mafic VMS deposits is not usually preserved because magmatic volatile influx decreases and is progressively overprinted and diluted by a seawater derived fluid signature during deposit maturation (Martin et al., 2020).

In addition to an enrichment in volatile elements, low S-isotope ratios in sulfide (<-2‰) and sulfate minerals (<+18‰) are generated during the disproportionation of SO_2 degassed from volatile-rich magmas in immature, subduction-influenced seafloor systems (e.g., McDermott et al., 2015). However, in active mafic SMS deposits that generally occur along mid-ocean ridges, the $\delta^{34}S$ composition of sulfide minerals is less-variable than subduction-influenced environments with the $\delta^{34}S$ composition of sulfide minerals falling between 0-10‰ (Hannington et al., 2005) indicating that sulfur was primarily sourced via thermochemical sulfate reduction (TSR) of seawater and through the leaching of sulfur from igneous lithologies (MORB; 0.1 ± 0.5‰ - Alt et al., 1993). Previous studies have shown that sulfur isotope systematics of Troodos VMS deposits are largely consistent with these processes with an average $\delta^{34}S$ composition in VMS deposit sulfide minerals of +4.6‰ ± 2.8‰ (1σ, n=220) and a range of -5.5 to +13.2‰ (Hannington et al., 1998; Keith et al., 2016b; Martin et al., 2020; Pedersen et al., 2017). Sulfur isotope values that are lighter than the magmatic mean (0-1‰; Alt, 1994) occur sporadically in several of the 25

77 Troodos VMS deposits that have been sampled in previous studies (Keith et al., 2016b, Martin et al., 2020).
78 These light sulfur isotope values have previously been interpreted as indicating an increased magmatic
79 volatile influx in these deposits (Keith et al., 2016b; Martin et al., 2020).

80 Here, we demonstrate that a volatile-rich signature has been identified in the Mala VMS deposit, which
81 we interpret as the rare and exceptionally preserved expression of an immature volatile-rich mafic hosted
82 VMS deposit. Sulfur isotope analysis of sulfate and sulfide minerals that retain primary seafloor textures,
83 that are very rarely preserved in ancient VMS deposits confirm that Mala experienced an elevated
84 magmatic volatile influx, resulting in low S-isotope ratios in sulfide and sulfate minerals with respect to the
85 Troodos magmatic mean (Alt, 1994) and Cretaceous seawater (Kampschulte and Strauss, 2004),
86 respectively. This signature is notably different from all other Troodos VMS deposits and other active and
87 ancient mafic VMS deposit analogues, suggesting that metals and sulfur are sourced from the direct
88 contribution of a magmatic volatile phase. Moreover, our data indicate an evolution in sulfide
89 geochemistry from volatile-rich with low S-isotope ratios, toward a volatile poor composition with a heavy
90 S-isotope signature, supporting previous studies focused on bi-modal VMS deposits that indicate a
91 transition in metal and sulfur source(s) with deposit maturation (Huston et al., 1995: Large, 1992; Martin
92 et al., 2020).

93 **2. Geological setting**

94 The Troodos ophiolite of Cyprus is Late Cretaceous in age (~92 Ma; Mukasa and Ludden, 1987) and formed
95 in a supra-subduction zone environment, most likely a nascent fore-arc type setting (Miyashiro, 1973;
96 Pearce and Robinson, 2010). Domical uplift in the Neogene focused under Mt. Olympus has led to the
97 exposure of a complete ophiolite stratigraphy consisting of mantle peridotites, cumulate ultramafics,
98 gabbro, plagiogranites, the sheeted dyke complex (SDC) and the extrusive sequence (Figure 1; Gass, 1968;
99 Simonian and Gass, 1978; Varga and Moores, 1985). Massive sulfide deposits that range in size from 0.05
100 to 15 Mt, with a typical grade of ~1.5 wt.% Cu (Hannington et al., 1998) occur at the periphery of the
101 ophiolite within the extrusive sequence. The distribution of these deposits is controlled by seafloor fault
102 networks that delineate three major graben structures that represent fossil spreading axes (Bettison-Varga

et al., 1992; Varga and Moores, 1985). From W-E these are; Solea, Mitsero and Larnaca grabens (Figure 1; Varga and Moores 1985).

2.1 The Mala VMS deposit

The Mala VMS deposit is located in SW Troodos within the Solea graben domain approximately 4.5 km E of Pano Panagia in the Pafos Forest region (047042-3864323, WGS 1984 - Figure 1). Mala is located deep in the lava stratigraphy at the basal-lower pillow lava (BG-LPL) transition (Figure 2A). The exposed deposit comprises a massive pyrite mound measuring approximately 8 x 12 m (width x height) (Figure 2A) that extends for ~100 m along strike with historic extraction of 200,000 tonnes of pyrite ore grading 0.45% Cu and 0.3% Zn (Brazilian Metals Group, 2013). The mound that is sampled in this study has a crudely banded appearance (Figure 2A and A1) containing abundant pyrite and gypsum. The mound is capped by a thin veneer (<2 m) of altered lava that indicates the burial of the VMS mound whilst it was still active (Figure 2A1 and B). Lava flows enclosing the mound are less-altered than the lavas directly above the mound and locally contain mordenite and natrolite that are common throughout the Troodos lava stratigraphy (Gass and Smewing, 1973). Within the VMS mound are crude laminations of fine-grained gypsum (10-60 cm thick) that occur parallel to the mound margins (Figure 2C-F). Gypsum is intergrown with disseminated euhedral pyrite (Figure 2C). Gypsum veins also occur in surrounding wall-rock associated with disseminated pyrite (Figure 2F). Pyrite occurs in three distinct textures within the Mala mound; massive (Figure 2G and I), dendritic (Figure 2G and H) and as disseminated grains (Figure 2I). Disseminated pyrite forms within gypsum and surrounding wall-rock (Figure 2C and F) whilst massive and dendritic varieties occur in discrete pods (Figure 2A1 and E). The Mala VMS deposit remains of economic interest and has recently been investigated by the Brazilian Metals Group (BMG) as a potential Cu-Zn prospect with drilling intersections of massive pyrite, sphalerite and chalcopyrite grading 1.16% Cu and 1.14% Zn over a thickness of 18 m (BMG, 2013).

3. Methods

3.1 Sulfur isotope analysis

Sulfur isotope ($\delta^{34}S$) analysis was performed at the Natural Environmental Research Council (NERC) stable isotope laboratory at the Scottish Universities Environmental Research Centre (SUERC). Analyses were performed on mineral separates that were optically checked for purity. Each analysis used approximately 4-5 mg of sample for pyrite and 10-12 mg for gypsum that was subsequently converted to SO_2 by combustion with 200 mg of cuprous oxide. The released SO_2 gas was then purified in a vacuum line utilising an acetone-CO_2 slush trap to remove water and a standard n-pentane trap to separate SO_2 from CO_2 following the method of Robinson and Kusakabe (1975). All SO_2 samples were analysed using a VGA SIRA II gas source mass spectrometer at SUERC. Values are calculated relative to the Vienna-Canyon Diablo Troilite (V-CDT) reference material and are reported in standard notation (‰). Reproducibility was monitored through the analysis of standards NBS-123 (+17.1‰), IAEA-S-3 (-31.5‰), SUERC's internal standard CP-1 (-4.6‰), NBS 127 (+20.3‰) and SUERC's internal standard BIS (+27.2‰). Reproducibility is reported as better than 0.7‰ (1σ) for all analyses (see Appendix 1).

3.2 Trace element geochemistry

Laser Ablation ICP-MS (LA-ICP-MS) was used to determine the *in situ* trace element composition of pyrite. Measurements were carried out at Cardiff University utilising a New Wave Research UP213 UV laser coupled to an iCAP RQ ICP-MS. Spot analyses were performed with a nominal spot size of 55 µm in time-resolved analysis mode at a frequency of 10 Hz. Acquisition lasted 45 seconds and a gas blank was measured for 20 seconds prior to ablation. Subtraction of gas blanks and internal standard corrections were performed using Thermo Plasmalab software. The repeated analysis of UQAC FeS-1 during the laser ablation study yielded <10% relative standard deviation (RSD) for Co, As, Se, Ag, Pb and Bi and between 10-18% RSD for Cu, Zn, Sb, Te and Au. RSD for Cd was 26% (Appendix 2). For all analyses, ^{33}S was used as an internal standard. A stoichiometric value of 53.5 wt.% S was used for all analyses and is within error of measured values for pyrite from Troodos VMS deposits (Martin et al., 2019).

4. Results

4.1 Sample characterisation

Both sulfide and sulfate minerals were sampled (Figure 2A-F; see Appendix 3). Towards the top of the VMS mound is a massive fine-grained (2-3 mm) gypsum horizon that is approximately 60-80 cm thick, and contains coarse (1-2 cm) euhedral pyrite grains (Figure 2C). At the base of the mound, gypsum forms small 1-5 cm coalescing veins that form a mesh texture (Figure 2A1 and D). Gypsum also occurs infilling or cementing pyrite breccia. Pyrite primarily occurs in two morphologies in the sulfide mound; as massive pods that contained dendritic and massive euhedral textured pyrite (Figure 2E, G, H and I) and as disseminated grains within gypsum and surrounding mineralized wall-rock (Figure 2C, F and J). Samples in this study were collected throughout the entire exposed sulfide mound, and are representative of mound-scale hydrothermal processes (see Appendix 3).

4.2 Sulfur isotopes

We report the $\delta^{34}S$ composition of pyrite (n=28) and gypsum (n=26) from the Mala VMS deposit (Figure 3). The $\delta^{34}S$ composition of pyrite ranges from -7.6‰ to +0.1‰ with a median composition of -4.3 ± 1.9‰ (1σ, n=28; Figure 3). The largest depletion in ^{34}S of -7.6‰ occurs in disseminated pyrite hosted in the wall-rock surrounding the sulfide mound (Figure 2F and J). There is no systematic variation in the sulfur isotopic composition of pyrite across the mound (from E-W) or with stratigraphic depth from top to bottom (Appendix 3).

The sulfur isotopic composition of gypsum ranges from +10.2‰ to +18.1‰ with a median composition of +14.3 ± 2.1‰ (1σ, n=26; Figure 3). In some samples where both pyrite and gypsum co-exist (in hand specimen) fractionation between pyrite and gypsum was calculated ($\Delta^{34}S_{sulfate-sulfide}$) and ranges from 15.9‰ to 21.0‰ with a median value of 17.8‰ (n=6 pairs) (Appendix 1).

4.3 Trace elements in pyrite

Trace element geochemistry of pyrite from the Mala VMS mound (n=61) is highly variable. Pyrite contains high concentrations of magmatic volatile elements with average concentrations of Au, Cu, Te and Se of 1.2, 873, 40 and 878 ppm (n=61) (Figure 4). Selenium in pyrite ranges from 9,565 ppm to below the detection limit (~12 ppm) (Figure 4). Bismuth concentrations are low (<10 ppm) and do not exhibit any

correlation with Te (Figure 4). Notable correlation exists between Te and Se (R^2=0.67), Co and Se (R^2=0.85) and Ag and Au (R^2=0.79) (Figure 4).

5. Discussion

5.1 Preservation of sulfate-sulfide relationships

Primary mound-related sulfate minerals such as anhydrite are rarely preserved in ancient VMS deposits (Çagatay and Eastoe, 1995; Huston et al., 2011; Torró et al., 2018). This is especially true for Troodos VMS deposits where such large quantities of sulfate minerals, as we observe at Mala, have not been reported with the exception of minor gypsum at the Agrokipia B VMS deposit (Constantinou and Govett, 1973). This is due to the retrograde solubility of anhydrite in aqueous fluids <150˚C that leads to its dissolution upon cessation of hydrothermal activity within the sulfide mound (Blounot and Dickson, 1969; Mills et al., 1998; Ohmoto, 1996).

More commonly in ancient VMS deposits, especially felsic hosted deposits (Ohmoto, 1996), barite is preserved due to its extremely low solubility in seawater relative to anhydrite (Averyt and Paytan, 2003; Jamieson et al., 2016). At the Mt. Lyell VMS deposit (Australia) barite forms veinlets in wall-rocks or more rarely 1-2 cm thick veins associated with pyrite (Walshe and Solomon, 1981). At the Saf'yanovka VMS deposit (Urals) barite occurs cementing breccias or as aggregates associated with sulfide minerals (Safina et al., 2016).

Whilst no anhydrite or barite is preserved in the Mala mound, abundant gypsum persists. The gypsum is interpreted to have formed by the hydration of primary anhydrite that formed during hydrothermal activity in the Mala mound on the Cretaceous seafloor as sulfide-sulfate textural relationships are analogous to those observed in actively forming SMS deposits (Figure 5). Hydration of anhydrite to form gypsum was most likely driven by meteoric water infiltration during uplift and exposure of the deposit, however, further $\delta^{18}O$ and δD isotope analysis of gypsum would be needed to confirm this (Matsubaya and Sakai, 1973).

A burial depth of 0.5 ± 0.2 km has been suggested to optimise the preservation potential of VMS deposits in Troodos; at this depth seawater ingress is minimal and destruction of the VMS deposit by later cross-cutting dykes is reduced (Hall and Yang, 1994). However, this model fails to account for the effect of localised fault related fluid flow on VMS deposit preservation that would lead to the dissolution of anhydrite during low-temperature fluid interaction. Nevertheless, we suggest that the burial and sealing of the Mala VMS deposit whilst it was still hydrothermally active, as lavas above the exposed mound are highly altered (Figure 2B), was advantageous in the exceptional preservation of gypsum as it sealed the deposit from later off-axis low temperature fluid flow (Prichard and Maliotis, 1998). The exact mechanism of why and how gypsum was preserved in the Mala mound and not in other Troodos VMS deposits remains enigmatic.

The preservation of primary textural relationships between pyrite and sulfate minerals are rare in ancient VMS deposits compared with actively forming SMS deposits. In the Mala mound the preserved sulfide-sulfate relationships are comparable to textures recorded in active SMS deposits (e.g., TAG; Gemmell and Sharpe, 1998) (Figure 5). We sub-divide gypsum textures into (i) massive, (ii) veined (iii) mesh textured and (iv) brecciated morphologies (Figure 5). Towards the top of the VMS mound is a massive fine-grained (2-3 mm) gypsum horizon that is approximately 60-80 cm thick, and contains coarse (1-2 cm) euhedral pyrite grains (Figure 5A). At the base of the mound, gypsum forms small 1-5 cm coalescing veins that form a mesh texture (Figure 5B-C). Gypsum also occurs infilling or cementing pyrite breccia (Figure 5D). These relationships, preserved in a 90 million year old VMS deposit, are texturally analogous to known samples from active SMS deposits (Figure 3) (Gemmell and Sharpe, 1998; Humphris et al., 1995). Similar textural relationships between anhydrite-gypsum-barite and sulfide minerals are also rarely documented in ancient bi-modal and Kuroko VMS deposits where they are also interpreted as the preservation of hypogene seafloor textures (Cazañas et al., 2008; Eldridge et al., 1983; Ohmoto, 1996). Moreover, the preservation of dendritic and porous textured pyrite, both of which are common in SMS deposits, that do not exhibit any visible sign of recrystallization or oxidation, further support that pyrite textures are of seafloor origin and did not form via supergene replacement or recrystallization of earlier pyrite

generations (Grant et al., 2018; Herrington et al., 1998; Koski et al., 1984; Nozaki et al., 2016). Furthermore, the dissolution of anhydrite and later re-precipitation of secondary gypsum would form brecciated, vuggy or collapse textures as observed in other Troodos VMS deposits and this is not observed (Constantinou and Govett, 1973). Thus, our data indicate that sulfide-sulfate mineral relationships at Mala reflect primary mineralising processes that occurred on the Cretaceous seafloor. We use sulfur isotope analysis of pyrite and gypsum to further constrain the source(s) of sulfur in the Mala VMS deposit.

5.2 Assessing a variable magmatic volatile influx

5.2.1 Sulfur isotope systematics

Typically, in mafic hosted VMS deposits, metals are thought to be derived from the alteration of igneous rocks at high-temperatures >350°C during the formation of epidosites in the SDC (Jowitt et al., 2012; Patten et al., 2017; Richardson et al., 1987). In this scenario, both metals and sulfur are leached from the SDC during hydrothermal fluid circulation. VMS deposits formed via this processes are expected to preserve a $\delta^{34}S$ signature in sulfide minerals that reflect the variable sourcing of sulfur from TSR of seawater (+18-19‰ in the Cretaceous; Kampschulte and Strauss, 2004) and the leaching of primary magmatic sulfur/sulfide minerals (0-1‰, Troodos; Alt, 1994). In lower temperature environments (<120°C) microbial sulfate reduction (MSR) is an important process producing extremely light $\delta^{34}S$ values in sulfide minerals as low as -38.9‰, however, in high temperature hydrothermal fluids (>120°C) MSR is absent or a minor component (McDermott et al., 2020; Nozaki et al., 2020). This leads to an average $\delta^{34}S$ for sulfide minerals in all Troodos VMS deposits of +4.6‰ ± 2.8‰ (1σ)(Hannington et al., 1998; Keith et al., 2016b; Martin et al., 2020; Parvaz, 2004; Pedersen et al., 2017). The $\delta^{34}S$ composition of sulfate minerals in actively forming mafic hosted SMS deposits generally reflects the composition of ambient seawater sulfate (+21‰ present day; Rees et al., 1978). This reflects the localised mixing of hydrothermal fluids with seawater to produce anhydrite in the VMS mound and surrounding area (Mills et al., 1998). We use the sulfur isotopic composition of pyrite and its relationship to gypsum as a proxy for the original conditions that produced anhydrite and pyrite in the Mala VMS deposit.

253 At Mala, $\delta^{34}S$ in pyrite averages -3.8‰ ± 1.9‰ (1σ, n=28; Figure 3), which is considerably lighter than the
254 Troodos magmatic mean (~0‰; Alt, 1994) and 8.4‰ lighter than the average for other Troodos VMS
255 deposits (Figure 4). Thus, the Mala pyrite $\delta^{34}S$ signature is not compatible with our current understanding
256 of sulfur cycling in the Troodos ophiolite or mafic-hosted VMS deposits in general. Gypsum from the Mala
257 mound yields values ranging from +10.2 to +18.1‰ with an average of +14.5‰ ± 2.0‰ (1σ, n=26; Figure
258 3). These values are dominantly lighter than Cretaceous seawater sulfate (+18-19; Kampschulte and
259 Strauss, 2004) indicating that the sulfur was not just sourced directly from local seawater, which is typically
260 observed in active mid-ocean ridge hosted SMS deposits (Chiba et al., 1998; Kusakabe et al., 1982). Nor
261 are the sulfur isotope data compatible with the formation of gypsum during sulfide weathering or during
262 oxidation of sulfides during the waning stages of hydrothermal activity (Çagatay and Eastoe, 1995; Glynn
263 et al., 2006), which would produce $\delta^{34}S$ values in gypsum similar to pyrite. Secondary veins of gypsum that
264 cross-cut massive sulfide at the Skouriotissa VMS deposit in Troodos average +6.6‰, a $\delta^{34}S$ value that is
265 indistinguishable from hypogene sulfide minerals (Parvaz, 2004). Furthermore, measured $\delta^{34}S$ values from
266 gypsum at Mala are indistinguishable from values for magmatic sulfate analysed in Troodos plagiogranites
267 at +12.3‰ (Kawahata et al., 1997). Additional sulfur sources, such as sediment interaction and Miocene
268 evaporites, can be discounted as the Troodos ophiolite formed in a sediment-free environment and
269 gypsum formation during later uplift and exposure related fluid flow (e.g., Miocene evaporites) would lead
270 to an enrichment in $\delta^{34}S$ to approximately +22‰ (Alt, 1994) and this is not observed (Figure 6).

271 The light $\delta^{34}S$ values in sulfide and sulfate minerals, with respect to primary magmatic sulfur and
272 Cretaceous seawater sulfate respectively, are attributed to a SO_2-rich magmatic fluid or vapour that has
273 undergone disproportionation via the reaction(s) (Holland, 1965; Kusakabe et al., 2000):

274 $$3SO_2 + 2H_2O = 2H_2SO_4^- + S^0 + 2H^+ \quad (1)$$

275 $$4SO_2 + 4H_2O = 3HSO_4^- + H_2S + 3H^+ \quad (2)$$

276 Reaction 2 (equation 2), which produces H_2S, occurs preferentially over reaction 1 (equation 1) in more
277 reducing, high-temperature fluids in systems with low total sulfur (Kusakabe et al., 2000). Native sulfur is
278 absent in the Mala VMS mound and surrounding rocks, indicating that fluids were reducing and high-

279 temperature (>350°C), and that reaction 2 prevailed. Fractionation between SO_4^{2-} and H_2S leads to
280 enrichment of ^{34}S in SO_4^{2-} and corresponding depletion of ^{34}S in H_2S relative to the initial bulk sulfur isotopic
281 composition (i.e. 0-1‰ for Troodos; Figure 6) (Kusakabe et al., 2000; Ohmoto and Lasaga, 1982; Rye, 2005),
282 consistent with the observed $\delta^{34}S$ in pyrite and gypsum at Mala (Figure 6).

283 Using the fractionation factor of Sakai (1968) pyrite-gypsum pairs from Mala (Appendix 1 and 3) yield
284 geologically reasonable average equilibrium temperatures of 381˚C (range = 318-462°C) for VMS deposit
285 formation. Furthermore, a sample located at the margin of the mound that is expected to experience lower
286 temperature fluid flow, yielded the lowest temperature of 318˚C (Appendix 2). For comparison, formation
287 temperatures estimated at the Skouriotissa VMS deposit are 411°C (Keith et al., 2016b), comparable to
288 the average of 381°C estimated for Mala. The highest temperature estimated in this study at Mala of 462˚C
289 perhaps indicates disequilibrium between some pairs (e.g., Hutchinson et al., 2020) as this temperature is
290 too high to have formed in the VMS mound where vent fluid temperatures are typically <400°C (Von
291 Damm, 1995). Moreover, at these high temperatures (>318°C) MSR of seawater can be discounted as a
292 potential source of reduced sulfur as MSR does not occur at temperatures >120°C (McDermott et al., 2020;
293 Takai et al., 2008).

294 The sulfur isotopic composition of gypsum at Mala indicates that sulfate formed via the disproportionation
295 of magmatic SO_2 with only a minor seawater sulfate component (Figure 6). This is distinctly different from
296 anhydrite sampled in mafic-hosted SMS deposits on mid-ocean ridges where sulfate minerals preserve the
297 $\delta^{34}S$ signature of ambient seawater sulfate (e.g., TAG or 21°N EPR; Chiba et al., 1998; Gemmell and Sharpe,
298 1998; Herzig et al., 1998b; Kusakabe et al., 1982). If all the sulfate at Mala was produced from
299 disproportionation of magmatic SO_2, the expected sulfate $\delta^{34}S$ value would be +10.5‰ at 350˚C, with a
300 range of +11.3 to +7.4‰ in the temperature range calculated previously (318-462°C) for Mala (Figure 6;
301 Sakai, 1968). The $\delta^{34}S$ in gypsum at Mala is slightly heavier than this (average = +14.5‰), indicating a
302 contribution of a ^{34}S enriched source of sulfur derived from seawater mixing within the mound (Figure 6).
303 However, this source is a minor component when compared to other mafic VMS deposits on mid-ocean
304 ridges (Figure 7).

305 During the disproportion of SO_2, highly acidic fluids are generated due to the production of H_2SO_4
306 (Kusakabe et al., 2000; Ohmoto and Lasaga, 1982; Seewald et al., 2015). Interaction with these highly acidic
307 fluids alter the surrounding rock to an advanced argillic mineral assemblage, such as those observed below
308 the seafloor at the Brothers NW Caldera (de Ronde et al., 2019) and DESMOS caldera (Gena et al., 2001).
309 No advanced argillic assemblage was observed surrounding the Mala VMS deposit as the VMS mound was
310 covered by lava flows after the accumulation of massive sulfide on the seafloor; hence, the wall-rocks
311 enclosing the deposit do not exhibit any evidence of high temperature (>300°C) alteration, instead
312 containing only zeolite minerals that formed during near-surface convection of seawater forming
313 mordenite and natrolite. However, we suggest that if advanced argillic alteration exists, it would be limited
314 to the stockwork zone immediately underlying the VMS mound as this region experiences the most intense
315 fluid flow during deposit formation, an area that is not currently exposed.

316 So far, evidence of disproportionation has only been recorded in the most immature deposits in a few
317 active subduction-related environments and in ancient deposits associated with bi-modal or felsic volcanic
318 successions and rarely in VMS deposits associated with mafic host rocks. Similar light $\delta^{34}S$ values in sulfide
319 and sulfate minerals occur in active SMS deposits such the Conical Seamount, Lihir (Gemmell et al., 2004),
320 PACMANUS, Manus back-arc basin (Kim et al., 2011; Roberts et al., 2003), SuSu Knolls, Manus back-arc
321 basin (Yeats et al., 2014) and the Brothers Cone site, Kermadec arc (de Ronde et al., 2005; 2011)(Figure 7).
322 Moreover, light $\delta^{34}S$ values in sulfide minerals and more rarely sulfate minerals have also been reported
323 for ancient VMS deposits, for example the bi-modal Mt. Lyell VMS deposit (Australia), El Cobre VMS
324 deposit (Cuba) and the Romero VMS deposit (Dominican Republic), however the lighter $\delta^{34}S$ composition
325 of sulfate minerals is less-pronounced in these deposits compared to Mala (Cazañas et al., 2008; Torró et
326 al., 2018; Walshe and Solomon, 1981).

327 In Troodos VMS deposits, variation in sulfur source is demonstrated by comparing the $\delta^{34}S$ composition of
328 Mala pyrite with other Troodos VMS deposits (Hannington et al., 1998; Keith et al., 2016b; Martin et al.,
329 2020; Pedersen et al., 2017). To date, sulfide minerals from Troodos VMS deposits with a $\delta^{34}S$ composition
330 that is lighter than the Troodos magmatic mean (0-1‰; Alt, 1994) have only been identified in the

Skouriotissa and Sha VMS deposits in only a few isolated sulfide grains (Figure 7; Keith et al., 2016b; Martin et al., 2020). At Skouriotissa, deep stockwork pyrite has a $\delta^{34}S$ composition of -1.4‰, compared with shallow stockwork at +6.1‰ and massive sulfide samples at +4.8‰ (Keith et al., 2016b; Figure 7). At Sha an isolated pyrite grain with a $\delta^{34}S$ value of -5.5‰ was recorded, whilst all other samples averaged +2.8‰ (Martin et al., 2020). In both instances, a magmatic volatile influx and the disproportionation of SO_2 is inferred as the source of isotopically light sulfur in pyrite producing a $\delta^{34}S$ value that is below the Troodos magmatic mean (0-1‰; Alt, 1994).

A decrease in magmatic volatile influx with deposit maturity is suggested to explain the transition in $\delta^{34}S$ values from <0‰ in pyrite in immature VMS deposits to >0‰ in mature deposits (Herzig et al., 1998; Martin et al., 2020). In SMS deposits of the Valu Fa Ridge the youngest immature deposit, Hine Hina, that is located proximal to the subduction zone, is depleted in ^{34}S with an average $\delta^{34}S$ value of -5.2‰ in pyrite and +16.4‰ in barite (Herzig et al., 1998a). The most mature deposit (White Church) located distally to the subduction zone averages +4.8‰ in pyrite and +20.7‰ in barite (Herzig et al., 1998a; Figure 7). The magnitude of variation in $\delta^{34}S$ values in pyrite in Troodos VMS deposits is comparable to that observed in SMS deposits of the Valu Fa Ridge (Hine Hina, Vai Lili and White Church; Figure 7); representing both a decrease in magmatic volatile influx and an increase in seawater ingress with deposit maturation (Herzig et al., 1998a). At the Brothers volcano, the $\delta^{34}S$ composition of pyrite exhibits a systematic shift in composition towards heavy values with increasing age, further supporting variation in sulfur source with deposit maturity (de Ronde et al., 2011). In Troodos VMS deposits, the occurrence of isolated and randomly distributed light sulfur isotope values in some pyrite grains could indicate the preservation of an immature volatile-rich signature, indicating that magmatic volatile influx decreases with deposit maturation as seawater influx increases (Martin et al., 2020). The new data we present at Mala indicates a transition in sulfur source from one dominated by SO_2 disproportionation in immature VMS deposits, to TSR and the leaching of igneous sulfur in mature VMS deposits. The latter signature is reflected in the average $\delta^{34}S$ composition of sulfide minerals in Troodos VMS deposits of +4.6‰ (Martin et al., 2020).

Thus, we interpret the light sulfur isotope signature preserved in Mala pyrite and gypsum as representing an immature mafic VMS deposit with the $\delta^{34}S$ signature of the deposit transitioning towards heavier $\delta^{34}S$ values with increasing age, as preserved in other Troodos VMS deposits. We stress that the preservation of this immature sulfur isotope signature is exceptionally rare, out of 220 previously published $\delta^{34}S$ analyses from sulfide minerals in Troodos VMS deposits, spanning 25 individual deposits, only 3 values (excluding Mala) lie significantly (<-1‰) below the Troodos magmatic mean (Hannington et al., 1998; Keith et al., 2016b; Martin et al., 2020; Pedersen et al., 2017).

Sulfur isotope systematics in the Mala VMS deposit are distinctly different from all other Troodos VMS deposits. This primarily reflects the addition of sulfur from the disproportionation of SO_2 compared with the leaching of host rocks and TSR in other Troodos VMS deposits and mafic hosted VMS more widely (Gemmell and Sharpe, 1998; Hannington et al., 1998; Keith et al., 2016a,b; Martin et al., 2020; Pedersen et al., 2017). In addition to the light sulfur isotope composition of sulfide minerals, active and ancient VMS deposits that experienced an increased magmatic volatile influx may be variably enriched in Te, Se, Au, Cu, Bi and As due to their volatile nature (de Ronde et al., 2011; Hannington et al., 1999; Huston et al., 1995, 2011; Keith et al., 2016a; Layton-Matthews et al., 2008; Patten et al., 2020; Yang and Scott, 1996). If Mala did experience an increased magmatic volatile influx then an enrichment in these elements should be present.

5.2.2 Pyrite trace element geochemistry

Evidence of magmatic volatile influx in active and ancient VMS deposits is most prevalent in deposits that formed in a bi-modal or felsic environments such as those located in arcs and back-arc basins. In these environments magmas are volatile-rich and may contribute metals and sulfur to the overlying hydrothermal system (de Ronde et al., 2011; Hannington et al., 2005; Huston et al., 2011, 1995; Keith et al., 2016b; Ohmoto, 1996; Patten et al., 2020; Wohlgemuth-Ueberwasser et al., 2015).

Mala pyrite exhibits notable enrichments in Au, Cu, Te and Se relative to other Troodos VMS deposits (Figure 8A). Mala pyrite contains average concentrations of Au, Cu, Te and Se in pyrite of 1.2, 873, 40 and

878 ppm (n=61), respectively, whilst all other Troodos VMS deposits have average concentrations in pyrite of 0.3, 480, 7.2 and 178 ppm, respectively (n=1497; Martin et al., 2019, 2020) (Figure 8A). We suggest that the enrichment of Au, Cu, Te and Se indicates that Mala experienced an increased magmatic volatile influx relative to other Troodos VMS deposits. Se concentration and in particular Se/S ratios (expressed as Se/S $x10^6$) have been widely used as an indicator of magmatic volatile influx (Huston et al., 1995; Layton-Matthews et al., 2008). At Mala, we report the highest Se concentration in pyrite of 9,565 ppm, a concentration that is notably higher than the maximum reported in pyrite from the Se-rich Skouriotissa and Apkili VMS deposits at 1,886 ppm and 4,953 ppm, respectively (Keith et al., 2016b; Martin et al., 2020). This concentration is also notably higher than the maximum Se concentration measured in active subduction-influenced vent sites for example pyrite at the Brothers volcano (max = 4,102 ppm) or Hine Hina (max = 121 ppm) (Keith et al., 2016a). Consequently, this leads to Se/S ratios in pyrite at Mala that average 1,641 (maximum = 17,879), this is well above the suggested magmatic threshold of >500, further supporting the addition of magmatic volatiles in the Mala VMS deposit (Layton-Matthews et al., 2008).

Typically, mafic hosted hydrothermal systems such as those preserved in Troodos are considered as volatile-poor relative to subduction-influenced environments that contain both felsic and mafic lithologies (Hannington et al., 2005). In addition to an enrichment in certain metals, correlation between magmatic volatile elements at Mala is distinctly different from a typical Troodos VMS deposit (Figure 8B and C) where Te-Se exhibit no correlation (R^2= <0.05; Martin et al., 2019). At Mala they exhibit a moderate positive correlation (R^2=0.67; Figure 8B), suggesting a coupled relationship between Te-Se, possibly related to their volatile nature and common source (Huston et al., 1995; Keith et al., 2018a). Furthermore, we suggest that a strong positive correlation between Se and Co (R^2=0.85; Figure 8C) and a moderate positive correlation between Co and Te (not shown; R^2=0.62) possibly represents evidence of a renewed pulse of magmatic volatile-rich fluid into the Mala hydrothermal system. From observations in active systems, a renewed magmatic influx can cause an increase in vent fluid temperature and volatile species in the vent fluid such as H_2S (cf. Butterfield et al., 2011, 1994; Von Damm et al., 1995). At Mala, we suggest that an increase in Co concentration in pyrite is evidence for an increase in fluid temperature as Co is enriched in high-

temperature zones of active SMS deposits (e.g., TAG; Grant et al., 2018) and ancient Troodos VMS deposits (e.g., Skouriotissa; Keith et al., 2016b). Thus, a strong correlation between volatile elements Se-(Te) and Co could indicate the introduction of a renewed magmatic volatile phase into the hydrothermal system at Mala.

We suggest that differences in the trace element signature of pyrite between Mala and other Troodos VMS deposits are related to an increased magmatic contribution at Mala that decreases with deposit maturity, explaining the lower concentrations of Au, Cu, Te and Se in pyrite from other Troodos VMS deposits. A similar trend in Au enrichment in active SMS deposits is observed where deposits located in immature back-arc rifts contain elevated concentrations of Au relative to deposits in mature back-arcs, suggesting a decrease in the contribution of Au from magmatic volatiles with deposit maturity (Herzig and Hannington, 1995).

In Troodos VMS deposits, pyrite could undergo zone refining (Goldfarb et al., 1983) leading to remobilisation and expulsion of volatile metals in mature deposits if "over zone refining" occurred; a process suggested for the TAG SMS deposit (Hanninton et al., 1998). However, the effect of zone refining on trace metals such as Te and Se remains poorly characterised. The initial volatile-rich signature in pyrite could also be diluted during the growth of the sulfide mound. As the mound grows, immature, volatile-rich pyrite becomes fragmented and is cross-cut by later volatile-poor mature pyrite generations leading to the preservation of small areas of immature pyrite in a larger deposit; similar to the isolated immature pyrite grains with light $\delta^{34}S$ values (<0‰) previously analysed at the Sha and Skouriotssa VMS deposits (Keith et al., 2016b; Martin et al., 2020).

5.3 Implications for mafic VMS deposits

The Mala VMS deposit provides the rare opportunity to study sulfide-sulfate relationships in an immature VMS deposit that are otherwise generally only preserved in active systems. The exceptional preservation of seafloor sulfide-sulfate relationships at Mala demonstrates a robust link between light sulfur isotope values in pyrite and gypsum and Au, Cu, Te and Se enrichment in an ancient mafic VMS analogue, indicating

a magmatic volatile dominated source (Figure 9). So far, hydrothermal processes such as volatile influx and disproportionation of SO_2 have only been recognised in active and ancient, bi-modal or felsic hosted, subduction-influenced environments. The magmatic volatile contribution in basaltic/basaltic-andesite hosted VMS deposits is expected to be minor in comparison to bi-modal or felsic hosted deposits, due to a lower volatile content of the magma (Wallace, 2005; Wyllie 1979), however, data from the Mala VMS deposit demonstrates the significance of a magmatic volatile phase as an additional source of metal and sulfur in a mafic-hosted VMS deposit, a processes that had not previously been recognised in mafic VMS deposits (e.g., Huston et al., 1995). We suggest that the volatile-dominated signature preserved at Mala could represent the initial stage of VMS formation in basaltic/basaltic-andesite hosted mafic hydrothermal systems (Figure 9). This supports previously proposed models (Martin et al., 2020) that indicate a transition in metal source with VMS deposit maturity in mafic VMS deposits from an early magmatic volatile phase to epidotisation and host rock leaching with increasing maturity of the hydrothermal system (Figure 9), highlighting the significance of a magmatic volatile phase as a source of metal and sulfur in mafic VMS deposits. Mafic VMS deposits are conventionally considered as volatile poor, with ore forming processes analogous to mid-ocean ridge hosted SMS deposits (Hannington et al., 1998). Evidence from Mala, however, suggest that this is not universally true. The textural and geochemical similarities to modern SMS deposits presented here imply that Mala offers a new and readily accessible analogue to active SMS deposits in volatile-rich environments (Figure 9). Consequently, we propose that an initial enrichment in Au, Cu, Te and Se coupled with light $\delta^{34}S$ values in sulfide and sulfate minerals may be widespread in mafic VMS deposits but is rarely preserved.

As the hydrothermal system matures, seawater ingress increases and volatile influx decreases and is diluted, leading to the preservation of a “typical” mafic VMS deposit signature characterised by $\delta^{34}S$ >0‰ and a depletion in magmatic volatile elements in pyrite (especially Te, Se and Au). This mature isotopic signature is widely preserved in many Troodos VMS deposits where the average $\delta^{34}S$ composition of all sulfide minerals excluding Mala is +4.6‰ (n=220; Hannington et al., 1998; Keith et al., 2016b; Martin et al., 2020; Pedersen et al., 2017). This has important implications for the metal endowment of mafic VMS

458 deposits, suggesting that economically important metals such as Au, Cu and high-tech metals Te and Se
459 are initially enriched in pyrite in immature, low-tonnage deposits and decrease in concentration in pyrite
460 with time and system maturity. This leads to the preservation of localised and isolated grains of pyrite that
461 are enriched in volatile elements with a light $\delta^{34}S$ signature (<0‰) surrounded by volatile poor pyrite with
462 a $\delta^{34}S$ signature >0‰. This signature of enrichment could be widespread but not readily preserved or
463 sampled on the seafloor as actively forming deposits, and especially the interior of active SMS mounds are
464 relatively underexplored.

465 **5.4 Troodos as an analogue for actively forming mafic VMS deposits**

466 Ophiolite complexes such as Troodos are considered as the on-land type locality for actively forming mafic,
467 Cu-Zn or Cyprus-type VMS deposits (Barrie and Hannington, 1997; Franklin et al., 2005; Galley et al., 2007;
468 Herrington et al., 2005; Large, 1992; Piercey, 2011). However, it has long been recognised that ophiolites
469 do not represent fragments of oceanic crust formed at mid-ocean ridges, instead representing oceanic
470 crust that formed in a supra-subduction environment (e.g., fore arc; Miyashiro, 1973; Pearce and
471 Robinson, 2010). VMS deposits hosted in ophiolite terrains are considered analogous to actively forming
472 deposits that form along mid-ocean ridges, immature fore-arcs or mature back-arcs, for example the TAG
473 hydrothermal field on the MAR (Hannington et al., 1998; Piercey, 2011). These environments consist
474 dominantly of mafic lithologies (basalts) with a minor or absent felsic component (Barrie and Hannington,
475 1997; Galley et al., 2007; Piercey, 2011).

476 In this study we provide compelling isotopic and geochemical evidence that ore forming processes in some
477 ophiolite hosted VMS deposits are comparable to SMS deposits forming along immature back-arc rifts
478 (e.g., Hine Hina; Herzig et al., 1998a). This has important implications for metal enrichment in ophiolites,
479 most notably the significance of a magmatic volatile phase as a potential source of metals in mafic VMS
480 deposits that until now has only been widely documented in SMS/VMS deposits associated with bi-modal
481 lithologies (Keith et al., 2016b; Martin et al., 2020, 2019; Patten et al., 2020). Whilst this magmatic volatile
482 dominated signature is by no means unique to the Mala VMS deposit, occurring in ancient (Huston et al.,
483 2011) and actively forming bi-modal or felsic hosted deposits (de Ronde et al., 2011b Herzig et al., 1998a

484 Yeats et al., 2014), it has rarely been recognised in ancient or actively forming mafic-hosted VMS deposits
485 (Hannington et al., 1998; Keith et al., 2016a; Martin et al., 2020). This reflects the higher primarily volatile
486 content of magmas generated in subduction zones relative to mid-ocean ridge environments (cf. Wallace,
487 2005) and the ability of these melts to reach volatile saturation and contribute metals to the overlying
488 hydrothermal systems (de Ronde et al., 2005; Huston et al., 2011; Keith et al., 2018a; Patten et al., 2020;
489 Sun et al., 2004; Yang and Scott, 1996, 2002).

490 It is widely accepted that the Troodos ophiolite formed in a supra-subduction zone environment and not
491 at a mid-ocean ridge (Miyashiro, 1973; Muenow et al., 1990; Rautenschlein et al., 1985), most likely
492 representing a nascent fore-arc setting (Pearce and Robinson, 2010). This is in line with elevated H_2O
493 contents (Cameron, 1985; Fonseca et al., 2017; Muenow et al., 1990) and the more oxidizing nature of
494 Troodos melts relative to mid-ocean ridge basalts (FMQ +1.5; Jenner et al., 2010; Patten et al., 2017).
495 Furthermore, the composition of Troodos lava is different from mid-ocean ridge environments that are
496 generally basaltic, Troodos contains a suite of lithologies ranging from picrite to basaltic-andesite and
497 minor dacite (Cameron, 1985; Rautenschlein et al., 1985). Additionally, plagiogranite intrusions contain
498 magmatic brine inclusions indicating the possible exsolution of a magmatic volatile phase (Kelley et al.,
499 1992; Kelley and Früh-Green, 2000; Kelley and Robinson, 1990) that may have formed a source of metals
500 in overlying VMS deposits (Martin et al., 2020).

501 Therefore, caution should be exercised when comparing between ophiolite hosted VMS deposits and
502 actively forming mafic hosted SMS deposits, especially those hosted in mid-ocean ridge environments.
503 Despite the affiliation of Troodos VMS deposits with mafic lithologies, Mala demonstrates that the source
504 and processes that control metal enrichment in some mafic VMS deposits may be more analogous to
505 processes recognised in bi-modal subduction-influenced environments and not mid-ocean ridges, or that
506 a magmatic volatile source of metals is also present in mid-ocean ridge hosted SMS deposits but is rarely
507 detected or indeed preserved.

508 **6. Summary and Conclusions**

In this study we demonstrate the significance of magmatic volatiles as a potential source of metals and sulfur in mafic VMS deposits. We show that in an environment that is typically considered as being volatile poor, that the disproportionation of magmatic SO_2 is the principal source of sulfur in an immature mafic VMS deposit. This signature is exceptionally preserved in the Mala VMS mound where the average sulfur isotope composition of pyrite is -3.8‰ and gypsum +14.5‰; this is significantly less than the Troodos magmatic mean and Cretaceous seawater, respectively. Previously, such a sulfur isotopic signature has only been observed in ancient bi-modal hosted VMS deposits and in immature active SMS deposits in arc and back-arc basins. Here, we demonstrate that the influx of magmatic volatiles is responsible for the enrichment of Se, Te, Au and Cu in pyrite during the initial stages of VMS deposit formation. As the VMS deposit matures the initial volatile-rich signature is overprinted and diluted, hence it may be widespread in actively forming and ancient mafic-hosted VMS deposits but is rarely preserved.

ACKNOWLEDGMENTS

This work is funded by Natural Environmental Research Council (NERC) grant NE/M010848/1 awarded to Cardiff University. Isotope analyses was supported by NERC Isotope Geosciences Facilities Steering Committee grant IP-1766-1117. Alison McDonald is kindly acknowledged for her assistance during sulfur isotope analysis. We kindly thank Costas Constantinou and Andreas Zissimos at the Geological Survey Department of Cyprus for their continued support and enthusiasm toward this research. Michael Green and Ifigenia Gavriel are thanked for their assistance in the field. We thank Brian McNulty and an anonymous reviewer for their thoughtful and constructive reviews and Editor-in-chief Don Porcelli for the efficient editorial handling of this manuscript.

REFERENCES:

Alt, J.C., 1994. A sulfur isotopic profile through the Troodos ophiolite, Cyprus: Primary composition and the effects of seawater hydrothermal alteration. Geochim. Cosmochim. Acta 58, 1825–1840. https://doi.org/10.1016/0016-7037(94)90539-8

534 Alt, J.C., Shanks, W.C., Jackson, M.C., 1993. Cycling of sulfur in subduction zones: The geochemistry of
535 sulfur in the Mariana Island Arc and back-arc trough. Earth Planet. Sci. Lett. 119, 477–494.
536 https://doi.org/10.1016/0012-821X(93)90057-G
537 Anderson, M.O., Hannington, M.D., McConachy, T.F., Jamieson, J.W., Anders, M., Wienkenjohann, H.,
538 Strauss, H., Hansteen, T., Petersen, S., 2019. Mineralization and Alteration of a Modern Seafloor
539 Massive Sulfide Deposit Hosted in Mafic Volcaniclastic Rocks. Economic Geology 114, 857–896.
540 https://doi.org/10.5382/econgeo.4666
541 Arnold, M., Sheppard, S.M.F., 1981. East Pacific Rise at latitude 21°N: isotopic composition and origin of
542 the hydrothermal sulphur. Earth Planet. Sci. Lett. 56, 148–156. https://doi.org/10.1016/0012-
543 821X(81)90122-9
544 Averyt, K.B., Paytan, A., 2003. Empirical partition coefficients for Sr and Ca in marine barite: Implications
545 for reconstructing seawater Sr and Ca concentrations. Geochem. Geophys. Geosystems 4, 1-14
546 https://doi.org/10.1029/2002GC000426
547 Barrie, C.T., Hannington, M.D., 1997. Classification of Volcanic-Associated Massive Sulfide Deposits Based
548 on Host-Rock Composition, in: Volcanic Associated Massive Sulfide Deposits: Processes and
549 Examples in Modern and Ancient Settings. Society of Economic Geologists, pp. 1-11.
550 https://doi.org/10.5382/Rev.08.01
551 Wyllie, P.J., 1979. Magmas and volatile components. Am. Mineral. 64, 469–500.
552 Beaudoin, G & Therrien, P. (2009) The updated web stable isotope fractionation calculator. In: Handbook
553 of stable isotope analytical techniques, Volume-II. De Groot, P.A. (ed.). Elsevier: 1120-1122.
554 Bettison -Varga, L., Varga, R.J., Schiffman, P., 1992. Relation between ore-forming hydrothermal systems
555 and extensional deformation in the Solea graben spreading centre, Troodos ophiolite, Cyprus.
556 Geology 20, 987–990. https://doi.org/10.1130/0091-7613(1992)020<0987:RBOFHS>2.3.CO;2
557 Blounot, C.W., Dickson, F.W., 1969. The solubility of anhydrite (CaSO4) in NaCl-H 2O from 100 to 450°C
558 and 1 to 1000 bars. Geochim. Cosmochim. Acta 33, 227–245. https://doi.org/10.1016/0016-
559 7037(69)90140-9

560 Brazilian Metals Group, 2013. High-Grade Copper-Zinc Sulphide Mineralisation Identified At Mala
561 Prospect – Vrechia. < http://www.bmgl.com.au/investors/annual-reports.html> accessed
562 30/07/2018.
563 Butterfield, D.A., McDuff, R.E., Mottl, M.J., Lilley, M.D., Lupton, J.E., Massoth, G.J., 1994. Gradients in the
564 composition of hydrothermal fluids from the Endeavour segment vent field: Phase separation
565 and brine loss. J. Geophys. Res. Solid Earth 99, 9561–9583. https://doi.org/10.1029/93JB03132
566 Butterfield, D.A., Nakamura, K., Takano, B., Lilley, M.D., Lupton, J.E., Resing, J.A., Roe, K.K., 2011. High
567 SO2 flux, sulfur accumulation, and gas fractionation at an erupting submarine volcano. Geology
568 39, 803–806. https://doi.org/10.1130/G31901.1
569 Çagatay, M.N., Eastoe, C.J., 1995. A sulfur isotope study of volcanogenic massive sulfide deposits of the
570 Eastern Black Sea province, Turkey. Miner. Deposita 30, 55–66.
571 https://doi.org/10.1007/BF00208877
572 Cameron, W.E., 1985. Petrology and origin of primitive lavas from the Troodos ophiolite, Cyprus. Contrib.
573 Mineral. Petrol. 89, 239–255. https://doi.org/10.1007/BF00379457
574 Cazañas, X., Alfonso, P., Melgarejo, J.C., Proenza, J.A., Fallick, A.E., 2008. Geology, fluid inclusion and
575 sulphur isotope characteristics of the El Cobre VHMS deposit, Southern Cuba. Miner. Deposita
576 43, 805. https://doi.org/10.1007/s00126-008-0197-z
577 Chiba, H., Uchiyama, N., Teagle, D. A. H., 1998. Stable isotope study of anhydrite and sulfide minerals at
578 the TAG hydrothermal mound, Mid-Atlantic Ridge, 26°N. Proc. Ocean Drill. Program Sci. Results
579 158, 85–90.
580 Constantinou, G., Govett, G.J.S., 1973. Geology, geochemistry, and genesis of Cyprus sulfide deposits.
581 Econ. Geol. 68, 843–858. https://doi.org/10.2113/gsecongeo.68.6.843
582 de Ronde, C.E.J. de, Humphris, S.E., Höfig, T.W., Reyes, A.G., 2019. Critical role of caldera collapse in the
583 formation of seafloor mineralization: The case of Brothers volcano. Geology 47, 762–766.
584 https://doi.org/10.1130/G46047.1
585 de Ronde, C.E.J., Massoth, G.J., Butterfield, D.A., Christenson, B.W., Ishibashi, J., Ditchburn, R.G.,
586 Hannington, M.D., Brathwaite, R.L., Lupton, J.E., Kamenetsky, V.S., Graham, I.J., Zellmer, G.F.,

587 Dziak, R.P., Embley, R.W., Dekov, V.M., Munnik, F., Lahr, J., Evans, L.J., Takai, K., 2011. Submarine
588 hydrothermal activity and gold-rich mineralization at Brothers Volcano, Kermadec Arc, New
589 Zealand. Miner. Deposita 46, 541–584. https://doi.org/10.1007/s00126-011-0345-8
590 de Ronde, C.E.J. de, Hannington, M.D., Stoffers, P., Wright, I.C., Ditchburn, R.G., Reyes, A.G., Baker, E.T.,
591 Massoth, G.J., Lupton, J.E., Walker, S.L., Greene, R.R., Soong, C.W.R., Ishibashi, J., Lebon, G.T.,
592 Bray, C.J., Resing, J.A., 2005. Evolution of a Submarine Magmatic-Hydrothermal System: Brothers
593 Volcano, Southern Kermadec Arc, New Zealand. Econ. Geol. 100, 1097–1133.
594 https://doi.org/10.2113/gsecongeo.100.6.1097
595 Eldridge, C.S., Barton, P.B., Jr., Ohmoto, H., 1983a. Mineral Textures and Their Bearing on Formation of
596 the Kuroko Orebodies, in: Ohmoto, H., Skinner, B.J. (Eds.), The Kuroko and Related Volcanogenic
597 Massive Sulfide Deposits. Society of Economic Geologists
598 https://doi.org/10.5382/Mono.05.15
599 Fonseca, R.O.C., Kirchenbaur, M., Ballhaus, C., Münker, C., Zirner, A., Gerdes, A., Heuser, A.,
600 Botcharnikov, R., Lenting, C., 2017. Fingerprinting fluid sources in Troodos ophiolite complex
601 orbicular glasses using high spatial resolution isotope and trace element geochemistry. Geochim.
602 Cosmochim. Acta 200, 145–166. https://doi.org/10.1016/j.gca.2016.12.012
603 Franklin JM, Gibson HL, Galley AG, Jonasson IR (2005) Volcanogenic massive sulfide deposits. Econ. Geol.
604 100th Anniversary Volume. pp 523–560 https://doi.org/10.5382/AV100.17
605 Fuchs, S., Hannington, M.D., Petersen, S., 2019. Divining gold in seafloor polymetallic massive sulfide
606 systems. Miner. Deposita 54, 789–820. https://doi.org/10.1007/s00126-019-00895-3
607 Galley AG, Hannington M, Jonasson I (2007) Volcanogenic massive sulphide deposits. Mineral deposits
608 division. Geol Assoc Can Spec Publ 5:141–161
609 Gass, I.G., 1968. Is the Troodos Massif of Cyprus a Fragment of Mesozoic Ocean Floor? Nature 220, 39–
610 42. https://doi.org/10.1038/220039a0
611 Gass, I.G., Smewing, J.D., 1973. Intrusion, Extrusion and Metamorphism at Constructive Margins:
612 Evidence from the Troodos Massif, Cyprus. Nature 242, 26–29.
613 https://doi.org/10.1038/242026a0

614 Gemmell JB, Sharpe R (1998) Detailed sulfur-isotope investigation of the TAG hydrothermal mound and
615 stockwork zone, 26°N, Mid-Atlantic Ridge. Proc ODP, Sci Results 158:71-84
616 Gemmell, J.B., Sharpe, R., Jonasson, I.R., Herzig, P.M., 2004. Sulfur Isotope Evidence for Magmatic
617 Contributions to Submarine and Subaerial Gold Mineralization: Conical Seamount and the
618 Ladolam Gold Deposit, Papua New Guinea. Econ. Geol. 99, 1711–1725.
619 https://doi.org/10.2113/gsecongeo.99.8.1711
620 Gena, K., Mizuta, T., Ishiyama, D., Urabe, T., 2001. Acid-sulphate Type Alteration and Mineralization in
621 the Desmos Caldera, Manus Back-arc Basin, Papua New Guinea. Resour. Geol. 51, 31–44.
622 https://doi.org/10.1111/j.1751-3928.2001.tb00079.x
623 Glynn, S., Mills, R.A., Palmer, M.R., Pancost, R.D., Severmann, S. and Boyce, A.J., 2006. The role of
624 prokaryotes in supergene alteration of submarine hydrothermal sulfides. Earth Planet. Sci.
625 Lett., 244, 170-185.
626 Goldfarb, M.S., Converse, D.R., Holland, H.D., and Edmond, J.M., 1983.The genesis of hot spring deposits
627 on the East Pacific Rise, 21°N. Econ. Geol. Monogr., 5, 184-197.
628 Grant, H.L.J., Hannington, M.D., Petersen, S., Frische, M., Fuchs, S.H., 2018. Constraints on the behavior
629 of trace elements in the actively-forming TAG deposit, Mid-Atlantic Ridge, based on LA-ICP-MS
630 analyses of pyrite. Chem. Geol. 498, 45–71. https://doi.org/10.1016/j.chemgeo.2018.08.019
631 Hall, J.M., Yang, J.S., 1994. A preferred environment of preservation for volcanic massive sulfide deposits
632 in the Troodos Ophiolite (Cyprus). Econ. Geol. 89, 851–857.
633 https://doi.org/10.2113/gsecongeo.89.4.851
634 Hannington, M.D., Bleeker, W., Kjarsgaard, I., 1999. Sulfide Mineralogy, Geochemistry, and Ore Genesis
635 of the Kidd Creek Deposit: Part II. The Bornite Zone*, in: Hannington, Mark D., Barrie, C.T. (Eds.),
636 The Giant Kidd Creek Volcanogenic Massive Sulfide Deposit, Western Abitibi Subprovince,
637 Canada. Society of Economic Geologists, pp. 225-266 https://doi.org/10.5382/Mono.10.08
638 Hannington, M.D., de Ronde, C.D.J., Petersen, S., 2005. Sea-floor tectonics and submarine hydrothermal
639 systems, in: Hedenquist, J.W., Thompson, J.F.H., Goldfarb, R.J., Richards, J.P. (Eds.), Economic

Geology 100th Anniversary Volume. Society of Economic Geologists, Littleton, Colorado, USA, pp. 111–141.

Hannington, M.D., Galley, A.G., Herzig, P.M., Petersen, S., 1998. Comparison of the TAG mound and stockwork complex with Cyprus-type massive sulfide deposits. https://doi.org/10.2973/odp.proc.sr.158.217.1998

He, Y., Xiang, Y., Zhou, Y., Yang, Y., Zhang, J., Huang, H., Shang, C., Luo, L., Gao, J., Tang, L., 2018. Selenium contamination, consequences and remediation techniques in water and soils: A review. Environ. Res. 164, 288–301. https://doi.org/10.1016/j.envres.2018.02.037

Hedenquist, J.W., Lowenstern, J.B., 1994. The role of magmas in the formation of hydrothermal ore deposits. Nature 370, 519-527. https://doi.org/10.1038/370519a0

Herrington, R.J., Maslennikov, V.V., Spiro, B., Zaykov, V.V., Little, C.T.S., 1998. Ancient vent chimney structures in the Silurian massive sulphides of the Urals. Geological Society, London, Special Publications 148, 241–257. https://doi.org/10.1144/GSL.SP.1998.148.01.13

Herrington, R., Maslennikov, V., Zaykov, V., Seravkin, I., Kosarev, A., Buschmann, B., Orgeval, J.-J., Holland, N., Tesalina, S., Nimis, P., Armstrong, R., 2005. 6: Classification of VMS deposits: Lessons from the South Uralides. Ore Geol. Rev., 27, 203–237. https://doi.org/10.1016/j.oregeorev.2005.07.014

Herzig, P.M., Hannington, M.D., 1995. Polymetallic massive sulfides at the modern seafloor a review. Ore Geol. Rev. 10, 95–115. https://doi.org/10.1016/0169-1368(95)00009-7

Herzig, P.M., Hannington, M.D., Arribas A. Jr., 1998a. Sulfur isotopic composition of hydrothermal precipitates from the Lau back-arc: implications for magmatic contributions to seafloor hydrothermal systems. Miner. Deposita 33, 226–237. https://doi.org/10.1007/s001260050143

Herzig, P., Petersen, S. and Hannington, M.D., 1998b. Geochemistry and sulfur-isotopic composition of the TAG hydrothermal mound, Mid-Atlantic Ridge, 26 N. Proc. Ocean Drill. Program Sci. Results 158, 47–70.

665 Holland, H.D., 1965. Some applications of thermochemical data to problems of ore deposits; Part 2,
666 Mineral assemblages and the composition of ore forming fluids. Econ. Geol. 60, 1101–1166.
667 https://doi.org/10.2113/gsecongeo.60.6.1101

668 Humphris, S.E., Herzig, P.M., Miller, D.J., Alt, J.C., Becker, K., Brown, D., Brügmann, G., Chiba, H., Fouquet,
669 Y., Gemmell, J.B., Guerin, G., Hannington, M.D., Holm, N.G., Honnorez, J.J., Iturrino, G.J., Knott,
670 R., Ludwig, R., Nakamura, K., Petersen, S., Reysenbach, A.-L., Rona, P.A., Smith, S., A. A, S., Tivey,
671 M.K., Zhao, X., 1995. The internal structure of an active sea-floor massive sulphide deposit.
672 Nature 377, 713–716. https://doi.org/10.1038/377713a0

673 Huston, D.L., Relvas, J.M.R.S., Gemmell, J.B., Drieberg, S., 2011. The role of granites in volcanic-hosted
674 massive sulphide ore-forming systems: an assessment of magmatic–hydrothermal contributions.
675 Miner. Deposita 46, 473–507. https://doi.org/10.1007/s00126-010-0322-7

676 Huston, D.L., Sie, S.H., Suter, G.F., 1995. Selenium and its importance to the study of ore genesis: the
677 theoretical basis and its application to volcanic-hosted massive sulfide deposits using pixeprobe
678 analysis. Nucl. Instrum. Methods Phys. Res. Sect. B Beam Interact. Mater. At., Nuclear
679 Microprobe Technology and Applications 104, 476–480. https://doi.org/10.1016/0168-
680 583X(95)00462-9

681 Hutchison, W., Finch, A.A., Boyce, A.J., 2020. The sulfur isotope evolution of magmatic-hydrothermal
682 fluids: insights into ore-forming processes. Geochimica et Cosmochimica Acta 288, 176–198.
683 https://doi.org/10.1016/j.gca.2020.07.042

684 Jamieson, J.W., Hannington, M.D., Tivey, M.K., Hansteen, T., Williamson, N.M.-B., Stewart, M., Fietzke, J.,
685 Butterfield, D., Frische, M., Allen, L., Cousens, B., Langer, J., 2016. Precipitation and growth of
686 barite within hydrothermal vent deposits from the Endeavour Segment, Juan de Fuca Ridge.
687 Geochim. Cosmochim. Acta 173, 64–85. https://doi.org/10.1016/j.gca.2015.10.021

688 Jenner, F.E., O'Neill, H.S.C., Arculus, R.J., Mavrogenes, J.A., 2010. The Magnetite Crisis in the Evolution of
689 Arc-related Magmas and the Initial Concentration of Au, Ag and Cu. J. Petrol. 51, 2445–2464.
690 https://doi.org/10.1093/petrology/egq063

691 Jowitt, S.M., Jenkin, G.R.T., Coogan, L.A., Naden, J., 2012. Quantifying the release of base metals from
692 source rocks for volcanogenic massive sulfide deposits: Effects of protolith composition and
693 alteration mineralogy. J. Geochem. Explor. 118, 47–59.
694 https://doi.org/10.1016/j.gexplo.2012.04.005
695 Kampschulte, A., Strauss, H., 2004. The sulfur isotopic evolution of Phanerozoic seawater based on the
696 analysis of structurally substituted sulfate in carbonates. Chem. Geol., Applications of Stable
697 Isotope Techniques to Geological and Environmental Problems 204, 255–286.
698 https://doi.org/10.1016/j.chemgeo.2003.11.013
699 Fuchs, S., Hannington, M.D., Petersen, S., 2019. Divining gold in seafloor polymetallic massive sulfide
700 systems. Miner. Deposita 54, 789–820. https://doi.org/10.1007/s00126-019-00895-3
701 Kawahata, H., Kusakabe, M., Scott, S.D., 1997. Sulfate in plagiogranites from the Troodos ophiolite,
702 Cyprus. Geochem. J. 31, 119–124. https://doi.org/10.2343/geochemj.31.119
703 Keith, M., Haase, K.M., Klemd, R., Krumm, S., Strauss, H., 2016b. Systematic variations of trace element
704 and sulfur isotope compositions in pyrite with stratigraphic depth in the Skouriotissa volcanic-
705 hosted massive sulfide deposit, Troodos ophiolite, Cyprus. Chem. Geol. 423, 7–18.
706 https://doi.org/10.1016/j.chemgeo.2015.12.012
707 Keith, M., Haase, K.M., Klemd, R., Smith, D.J., Schwarz-Schampera, U., Bach, W., 2018a. Constraints on
708 the source of Cu in a submarine magmatic-hydrothermal system, Brothers volcano, Kermadec
709 island arc. Contrib. Mineral. Petrol. 173, 40. https://doi.org/10.1007/s00410-018-1470-5
710 Keith, M., Häckel, F., Haase, K.M., Schwarz-Schampera, U., Klemd, R., 2016a. Trace element systematics
711 of pyrite from submarine hydrothermal vents. Ore Geol. Rev. 72, 728–745.
712 https://doi.org/10.1016/j.oregeorev.2015.07.012
713 Keith, M., Smith, D.J., Jenkin, G.R.T., Holwell, D.A., Dye, M.D., 2018b. A review of Te and Se systematics in
714 hydrothermal pyrite from precious metal deposits: Insights into ore-forming processes. Ore Geol.
715 Rev. 96, 269–282. https://doi.org/10.1016/j.oregeorev.2017.07.023

716 Kelley, D.S., Früh-Green, G.L., 2000. Volatiles in mid-ocean ridge environments, in: Ophiolites and
717 Oceanic Crust: New Insights from Field Studies and the Ocean Drilling Program. Geol. Soc. Am.
718 https://doi.org/10.1130/0-8137-2349-3.237
719 Kelley, D.S., Robinson, P.T., 1990. Development of a brine-dominated hydrothermal system at
720 temperatures of 400–500°C in the upper level plutonic sequence, Troodos ophiolite, Cyprus.
721 Geochim. Cosmochim. Acta 54, 653–661. https://doi.org/10.1016/0016-7037(90)90361-N
722 Kelley, D.S., Robinson, P.T., Malpas, J.G., 1992. Processes of brine generation and circulation in the
723 oceanic crust: Fluid inclusion evidence from the Troodos Ophiolite, Cyprus. J. Geophys. Res. Solid
724 Earth 97, 9307–9322. https://doi.org/10.1029/92JB00520
725 Kim, J., Lee, K.-Y., Kim, J.-H., 2011. Metal-bearing molten sulfur collected from a submarine volcano:
726 Implications for vapor transport of metals in seafloor hydrothermal systems. Geology 39, 351–
727 354. https://doi.org/10.1130/G31665.1
728 Koski, R.A., Clague, D.A., Oudin, E., 1984. Mineralogy and chemistry of massive sulfide deposits from the
729 Juan de Fuca Ridge. GSA Bulletin 95, 930–945. https://doi.org/10.1130/0016-
730 7606(1984)95<930:MACOMS>2.0.CO;2
731 Kusakabe, M., Chiba, H., Ohmoto, H., 1982. Stable isotopes and fluid inclusion study of anhydrite from
732 the East Pacific Rise at 21°N. Geochem. J. 16, 89–95. https://doi.org/10.2343/geochemj.16.89
733 Kusakabe, M., Komoda, Y., Takano, B., Abiko, T., 2000. Sulfur isotopic effects in the disproportionation
734 reaction of sulfur dioxide in hydrothermal fluids: implications for the $\delta^{34}S$ variations of dissolved
735 bisulfate and elemental sulfur from active crater lakes. J. Volcanol. Geotherm. Res. 97, 287–307.
736 https://doi.org/10.1016/S0377-0273(99)00161-4
737 Large, R.R., 1992. Australian volcanic-hosted massive sulfide deposits: features, styles, and genetic
738 models. Econ. Geol. 87, 471–510. http://dx.doi.org/10.2113/gsecongeo.87.3.471
739 Layton-Matthews, D., Peter, J.M., Scott, S.D., Leybourne, M.I., 2008. Distribution, Mineralogy, and
740 Geochemistry of Selenium in Felsic Volcanic-Hosted Massive Sulfide Deposits of the Finlayson
741 Lake District, Yukon Territory, Canada. Econ. Geol. 103, 61–88.
742 https://doi.org/10.2113/gsecongeo.103.1.61

743 Martin, A.J., Keith, M., McDonald, I., Haase, K.M., McFall, K.A., Klemd, R., MacLeod, C.J., 2019. Trace
744 element systematics and ore-forming processes in mafic VMS deposits: Evidence from the
745 Troodos ophiolite, Cyprus. Ore Geol. Rev. 106, 205–225.
746 https://doi.org/10.1016/j.oregeorev.2019.01.024
747 Martin, A.J., Keith, M., Parvaz, D.B., McDonald, I., Boyce, A.J., McFall, K.A., Jenkin, G.R.T., Strauss, H.,
748 MacLeod, C.J., 2020. Effects of magmatic volatile influx in mafic VMS hydrothermal systems:
749 Evidence from the Troodos ophiolite, Cyprus. Chem. Geol. 531, 1-19.
750 https://doi.org/10.1016/j.chemgeo.2019.119325
751 Martin, A.J., McDonald, I., MacLeod, C.J., Prichard, H.M., McFall, K., 2018. Extreme enrichment of
752 selenium in the Apliki Cyprus-type VMS deposit, Troodos, Cyprus. Mineral. Mag. 82, 697–724.
753 https://doi.org/10.1180/mgm.2018.81
754 Matsubaya, O., Sakai, H., 1973. Oxygen and hydrogen isotopic study on the water of crystallization of
755 gypsum from the Kuroko type mineralization. Geochem. J. 7, 153–165.
756 https://doi.org/10.2343/geochemj.7.153
757 McDermott, J.M., Ono, S., Tivey, M.K., Seewald, J.S., Shanks, W.C., Solow, A.R., 2015. Identification of
758 sulfur sources and isotopic equilibria in submarine hot-springs using multiple sulfur isotopes.
759 Geochimica et Cosmochimica Acta 160, 169–187. https://doi.org/10.1016/j.gca.2015.02.016
760 McDermott, J.M., Sylva, S.P., Ono, S., German, C.R., Seewald, J.S., 2020. Abiotic redox reactions in
761 hydrothermal mixing zones: Decreased energy availability for the subsurface biosphere. PNAS
762 117, 20453–20461. https://doi.org/10.1073/pnas.2003108117
763 Mills, R.A., Teagle, D. a. H., Tivey, M.K., 1998. Fluid mixing and anhydrite precipitation within the TAG
764 mound. Oceanogr. Lit. Rev. 8, 1350.
765 Miyashiro, A., 1973. The Troodos ophiolitic complex was probably formed in an island arc. Earth Planet.
766 Sci. Lett. 19, 218–224. https://doi.org/10.1016/0012-821X(73)90118-0
767 Moss, R., Scott, S.D. and Binns, R.A., 2001. Gold content of eastern Manus basin volcanic rocks:
768 implications for enrichment in associated hydrothermal precipitates. Econ. Geol. 96, 91- 107.

769 Moss, R.L., Tzimas, E., Kara, H., Willis, P., Kooroshy, J., 2013. The potential risks from metals bottlenecks
770 to the deployment of Strategic Energy Technologies. Energy Policy 55, 556–564.
771 https://doi.org/10.1016/j.enpol.2012.12.053
772 Muenow, D.W., Garciat, M.O., Aggrey, K.E., Bednarz, U., Schmincke, H.U., 1990. Volatiles in submarine
773 glasses as a discriminant of tectonic origin: application to the Troodos ophiolite. Nature 343,
774 159–161. https://doi.org/10.1038/343159a0
775 Mukasa, S.B., Ludden, J.N., 1987. Uranium-lead isotopic ages of plagiogranites from the Troodos
776 ophiolite, Cyprus, and their tectonic significance. Geology 15, 825–828.
777 https://doi.org/10.1130/0091-7613(1987)15<825:UIAOPF>2.0.CO;2
778 Nozaki, T., Ishibashi, J.-I., Shimada, K., Nagase, T., Takaya, Y., Kato, Y., Kawagucci, S., Watsuji, T., Shibuya,
779 T., Yamada, R., Saruhashi, T., Kyo, M., Takai, K., 2016. Rapid growth of mineral deposits at
780 artificial seafloor hydrothermal vents. Scientific Reports 6, 22163.
781 https://doi.org/10.1038/srep22163
782 Nozaki, T., Nagase, T., Ushikubo, T., Shimizu, K., Ishibashi, J., and the D/V Chikyu Expedition 909
783 Scientists, 2020. Microbial sulfate reduction plays an important role at the initial stage of
784 subseafloor sulfide mineralization. Geology. https://doi.org/10.1130/G47943.1
785 Ohmoto, H., 1996. Formation of volcanogenic massive sulfide deposits: The Kuroko perspective. Ore
786 Geol. Rev., 10, 135–177. https://doi.org/10.1016/0169-1368(95)00021-6
787 Ohmoto, H., Lasaga, A.C., 1982. Kinetics of reactions between aqueous sulfates and sulfides in
788 hydrothermal systems. Geochim. Cosmochim. Acta 46, 1727–1745.
789 https://doi.org/10.1016/0016-7037(82)90113-2
790 Parvaz, D.B., 2014. Oxidation Zones of Volcanogenic Massive Sulphide Deposits in the Troodos Ophiolite,
791 Cyprus: Targeting Secondary Copper Deposits. PhD Thesis, University of Exeter.
792 Patten, C.G.C., Pitcairn, I.K., Alt, J.C., Zack, T., Lahaye, Y., Teagle, D.A.H., Markdahl, K., 2020. Metal fluxes
793 during magmatic degassing in the oceanic crust: sulfide mineralisation at ODP site 786B, Izu-
794 Bonin forearc. Miner. Deposita 55, 469–489. https://doi.org/10.1007/s00126-019-00900-9

795 Patten, C.G.C., Pitcairn, I.K., Teagle, D.A.H., 2017. Hydrothermal mobilisation of Au and other metals in
796 supra-subduction oceanic crust: Insights from the Troodos ophiolite. Ore Geol. Rev. 86, 487–508.
797 https://doi.org/10.1016/j.oregeorev.2017.02.019
798 Pearce, J.A., Robinson, P.T., 2010. The Troodos ophiolitic complex probably formed in a subduction
799 initiation, slab edge setting. Gondwana Res., A Tribute to Miyashiro 18, 60–81.
800 https://doi.org/10.1016/j.gr.2009.12.003
801 Pedersen, L.-E.R., Staudigel, H., McLoughlin, N., Whitehouse, M.J., Strauss, H., 2017. A multiple sulfur
802 isotope study through the volcanic section of the Troodos ophiolite. Chem. Geol. 468, 49–62.
803 https://doi.org/10.1016/j.chemgeo.2017.08.008
804 Piercey, S.J., 2011. The setting, style, and role of magmatism in the formation of volcanogenic massive
805 sulfide deposits. Miner. Deposita 46, 449–471. https://doi.org/10.1007/s00126-011-0341-z
806 Prichard, H.M., Maliotis, G., 1998. Gold mineralization associated with low-temperature, off-axis, fluid
807 activity in the Troodos ophiolite, Cyprus. J. Geol. Soc. 155, 223–231.
808 https://doi.org/10.1144/gsjgs.155.2.0223
809 Rautenschlein, M., Jenner, G.A., Hertogen, J., Hofmann, A.W., Kerrich, R., Schmincke, H.-U., White, W.M.,
810 1985. Isotopic and trace element composition of volcanic glasses from the Akaki Canyon, Cyprus:
811 implications for the origin of the Troodos ophiolite. Earth Planet. Sci. Lett. 75, 369–383.
812 https://doi.org/10.1016/0012-821X(85)90180-3
813 Rees, C.E., Jenkins, W.J., Monster, J., 1978. The sulphur isotopic composition of ocean water sulphate.
814 Geochim. Cosmochim. Acta 42, 377–381. https://doi.org/10.1016/0016-7037(78)90268-5
815 Roberts, S., Bach, W., Binns, R.A., Vanko, D.A., Yeats, C.J., Teagle, D. a. H., Blacklock, K., Blusztajn, J.S.,
816 Boyce, A.J., Cooper, M.J., Holland, N., McDonald, B., 2003. Contrasting evolution of hydrothermal
817 fluids in the PACMANUS system, Manus Basin: The Sr and S isotope evidence. Geology 31, 805–
818 808. https://doi.org/10.1130/G19716.1
819 Robinson, B.W., Kusakabe, Minoru., 1975. Quantitative preparation of sulfur dioxide, for sulfur-34/sulfur-
820 32 analyses, from sulfides by combustion with cuprous oxide. Anal. Chem. 47, 1179–1181.
821 https://doi.org/10.1021/ac60357a026

822 Rouxel, O., Fouquet, Y., Ludden, J.N., 2004. Subsurface processes at the lucky strike hydrothermal field,
823 Mid-Atlantic ridge: evidence from sulfur, selenium, and iron isotopes 1 1Associate editor: S.
824 Sheppard. Geochimica et Cosmochimica Acta 68, 2295–2311.
825 https://doi.org/10.1016/j.gca.2003.11.029
826 Rye, R.O., 2005. A review of the stable-isotope geochemistry of sulfate minerals in selected igneous
827 environments and related hydrothermal systems. Chem. Geol., 215, 5–36.
828 https://doi.org/10.1016/j.chemgeo.2004.06.034
829 Safina, N.P., Melekestseva, I.Yu., Nimis, P., Ankusheva, N.N., Yuminov, A.M., Kotlyarov, V.A., Sadykov,
830 S.A., 2016. Barite from the Saf'yanovka VMS deposit (Central Urals) and Semenov-1 and
831 Semenov-3 hydrothermal sulfide fields (Mid-Atlantic Ridge): a comparative analysis of formation
832 conditions. Miner. Deposita 51, 491–507. https://doi.org/10.1007/s00126-015-0617-9
833 Sakai, H., 1968. Isotopic properties of sulfur compounds in hydrothermal processes. Geochem. J., 2, 29–
834 49.
835 Seewald, J.S., Reeves, E.P., Bach, W., Saccocia, P.J., Craddock, P.R., Shanks, W.C., Sylva, S.P., Pichler, T.,
836 Rosner, M., Walsh, E., 2015. Submarine venting of magmatic volatiles in the Eastern Manus
837 Basin, Papua New Guinea. Geochim. Cosmochim. Acta 163, 178–199.
838 https://doi.org/10.1016/j.gca.2015.04.023
839 Simonian, K.O., Gass, I.G., 1978. Arakapas fault belt, Cyprus: A fossil transform fault. GSA Bull. 89, 1220–
840 1230. https://doi.org/10.1130/0016-7606(1978)89<1220:AFBCAF>2.0.CO;2
841 Stanton, R.L., 1984. Observations on the Appalachian-Caledonide ore province and their influence on the
842 development of stratiform ore genesis theory; a short historical review. Economic Geology 79,
843 1428–1441. https://doi.org/10.2113/gsecongeo.79.7.1428
844 Styrt, M.M., Brackmann, A.J., Holland, H.D., Clark, B.C., Pisutha-Arnond, V., Eldridge, C.S., Ohmoto, H.,
845 1981. The mineralogy and the isotopic composition of sulfur in hydrothermal sulfide/sulfate
846 deposits on the East Pacific Rise, 21°N latitude. Earth Planet. Sci. Lett. 53, 382–390.
847 https://doi.org/10.1016/0012-821X(81)90042-X

848 Sun, W., Arculus, R.J., Kamenetsky, V.S., Binns, R.A., 2004. Release of gold-bearing fluids in convergent
849 margin magmas prompted by magnetite crystallization. Nature 431, 975–978.
850 https://doi.org/10.1038/nature02972
851 Takai, K., Nakamura, K., Toki, T., Tsunogai, U., Miyazaki, M., Miyazaki, J., Hirayama, H., Nakagawa, S.,
852 Nunoura, T., Horikoshi, K., 2008. Cell proliferation at 122°C and isotopically heavy CH4
853 production by a hyperthermophilic methanogen under high-pressure cultivation. PNAS 105,
854 10949–10954. https://doi.org/10.1073/pnas.0712334105
855 Torró, L., Proenza, J.A., Espaillat, J., Belén-Manzeta, A.J., Román-Alday, M.C., Amarante, A., González, N.,
856 Espinoza, J., Román-Alpiste, M.J., Nelson, C.E., 2018. The Discovery of the Romero VMS Deposit
857 and Its Bearing on the Metallogenic Evolution of Hispaniola during the Cretaceous. Minerals 8,
858 507. https://doi.org/10.3390/min8110507
859 Varga, R.J., Moores, E.M., 1985. Spreading structure of the Troodos ophiolite, Cyprus. Geology 13, 846–
860 850. https://doi.org/10.1130/0091-7613(1985)13<846:SSOTTO>2.0.CO;2
861 Von Damm K.L. (1995) Controls on the chemistry and temporal variability of seafloor hydrothermal
862 fluids. Seafloor hydrothermal systems: Physical, chemical, biological, and geological interactions.
863 In: Humphris S.E., Zierenberg R.A., Mullineaux L.S., Thomson R.E. (eds) Seafloor hydrothermal
864 systems: physical, chemical, biological, and geological interactions. Geophys. Monogr., 91, Am
865 Geophys Union, Washington, DC, pp 222–247
866 Von Damm, K.L.., Oosting, S.E., Kozlowski, R., Buttermore, L.G., Colodner, D.C., Edmonds, H.N., Edmond,
867 J.M., Grebmeier, J.M., 1995. Evolution of East Pacific Rise hydrothermal vent fluids following a
868 volcanic eruption. Nature 375, 47–50. https://doi.org/10.1038/375047a0
869 Wallace, P.J., 2005. Volatiles in subduction zone magmas: concentrations and fluxes based on melt
870 inclusion and volcanic gas data. J. Volcanol. Geotherm. Res. 140, 217–240.
871 https://doi.org/10.1016/j.jvolgeores.2004.07.023
872 Walshe, J.L., Solomon, M., 1981. An investigation into the environment of formation of the volcanic-
873 hosted Mt. Lyell copper deposits using geology, mineralogy, stable isotopes, and a six-

874 component chlorite solid solution model. Econ. Geol. 76, 246–284.
875 https://doi.org/10.2113/gsecongeo.76.2.246
876 Williams-Jones, A.E., Heinrich, C.A., 2005. 100th Anniversary Special Paper: Vapor Transport of Metals
877 and the Formation of Magmatic-Hydrothermal Ore Deposits. Econ. Geol. 100, 1287–1312.
878 https://doi.org/10.2113/gsecongeo.100.7.1287
879 Wohlgemuth-Ueberwasser, C.C., Viljoen, F., Petersen, S., Vorster, C., 2015. Distribution and solubility
880 limits of trace elements in hydrothermal black smoker sulfides: An in-situ LA-ICP-MS study.
881 Geochim. Cosmochim. Acta 159, 16–41. https://doi.org/10.1016/j.gca.2015.03.020
882 Wyllie, P.J., 1979. Magmas and volatile components. Am. Mineral. 64, 469–500.
883 Yang, K., Scott, S.D., 2002. Magmatic Degassing of Volatiles and Ore Metals into a Hydrothermal System
884 on the Modern Sea Floor of the Eastern Manus Back-Arc Basin, Western Pacific. Econ. Geol. 97,
885 1079–1100. https://doi.org/10.2113/gsecongeo.97.5.1079
886 Yang, K., Scott, S.D., 1996. Possible contribution of a metal-rich magmatic fluid to a sea-floor
887 hydrothermal system. Nature 383, 420–423. https://doi.org/10.1038/383420a0
888 Yeats, C.J., Parr, J.M., Binns, R.A., Gemmell, J.B., Scott, S.D., 2014. The SuSu Knolls Hydrothermal Field,
889 Eastern Manus Basin, Papua New Guinea: An Active Submarine High-Sulfidation Copper-Gold
890 System. Econ. Geol. 109, 2207–2226. https://doi.org/10.2113/econgeo.109.8.2207
891

892 **FIGURE CAPTIONS**

893 **Figure 1:** Simplified map of the Troodos ophiolite, Cyprus. Dashed lines represent fossil spreading axes.
894 The Mala VMS deposit is located in the SW of the Massif. Inset image shows the location of the Troodos
895 ophiolite within the island of Cyprus (after Martin et al., 2018).

896 **Figure 2:** Field observations from the Mala VMS deposit. A) The exposed Mala massive sulfide mound
897 formed from crudely layered gypsum and pyrite. A1) Idealised stratigraphic section (not to scale) through
898 the Mala mound. *?? Probable location of advanced argillic alteration assemblage below the mound, an
899 area not currently exposed. Inset boxes and letters relate to the location of each subsequent image within

the mound. B) Altered volcanic veneer that overlies the Mala VMS mound and is approximately ~2 m thick. C) Massive bedded gypsum horizon (60-80 cm thick) surrounded by pyrite. C1 and C2) Euhedral pyrite in gypsum. D) Veined/mesh texture gypsum intergrown with pyrite. E) Massive pyrite lens containing abundant dendritic pyrite (see image G and I). F) Gypsum veins cross-cutting altered wall-rock that contains finely disseminated pyrite. G-J) Photomicrographs of pyrite in reflected light. G) Massive (Mas) and dendritic (Den) pyrite. H) Close-up image of dendritic pyrite. I) Typical massive pyrite with porous regions (left) overgrown by later euhedral pyrite (right). J) Disseminated euhedral pyrite within surrounding lava.

Figure 3: Sulfur isotope ($\delta^{34}S$) analysis of pyrite and gypsum from the Mala VMS mound (see Appendix 1 and 3 for sample location). Values in pyrite at Mala are below the Troodos Ophiolite magmatic mean of 0-1‰ (TO; Alt, 1994) and less-than other Troodos VMS pyrite (*Hannington et al., 1998; Keith et al., 2016b; Martin et al., 2020; Pederesen et al., 2017). Gypsum yields values between the Troodos magmatic mean and Cretaceous seawater (SW; Kampschulte and Strauss, 2004).

Figure 4: Pyrite chemistry analysed via LA-ICP-MS for the Mala VMS deposit. A) Te vs. Bi, B) Co vs. Se, C) Au vs. Ag, D) Te vs. Se. Dashed grey line represents the best fit regression line for presented data. Analyses that are below detection limit are taken as the detection limit (see Appendix 2).

Figure 5: Sulfide-sulfate relationships from the fossil Mala mound (A-D) and actively forming TAG deposit (A1-D1). Textures preserved in the Mala VMS mound are comparable to those found in active SMS deposits. A) Massive, bedded, fine-grained gypsum with euhedral pyrite. B) Veined gypsum containing fine-grained (<2 mm) disseminated euhedral pyrite. C) Mesh textured gypsum veins enclosing discrete pyrite pods. D) Breccia infill, sub-angular pyrite clasts cemented by gypsum. A1) Massive laminated anhydrite with finely disseminated pyrite. B1) Veined anhydrite with interstitial to crudely banded pyrite. C1) Pyrite with cross-cutting anhydrite veins. D1) Sub-angular pyrite clasts in an anhydrite matrix. GYP=gypsum, ANH=anhydrite, PY=pyrite (TAG images: ODP Leg 158, Hole 957C, Core 7N- photographed intervals in Appendix 4).

Figure 6: Sulfur isotope systematics for pyrite and gypsum at the Mala VMS deposit. Values in white boxes are the fractionation factors between SO_2 and pyrite/SO_4^{2-} at 350 and 400°C (Sakai, 1968). Grey boxes

indicate potential sulfur sources: Troodos (TO) magmatic mean (0-1‰; Alt, 1994), Cretaceous seawater (SW) (+18-19‰; Kampschulte and Strauss, 2004) and Miocene evaporites (+22‰; Alt, 1994). The expected fraction between SO_2 and pyrite/SO_4^{2-} at 350-400°C should produce pyrite with a $\delta^{34}S$ composition between -7.5‰ and -8.6‰ and sulfate between +8.9‰ and 10.5‰. Values at Mala are heavier than expected if disproportionation was the *only* source of sulfur.

Figure 7: Sulfur isotope composition of sulfide and sulfate minerals from Troodos VMS deposits, arc and back-arc basin hosted SMS deposits and mid-ocean ridge SMS deposits. Light values <0‰ occur at Mala and only rarely in other Troodos VMS deposits at Skouriotissa and Sha. Arc/back-arc basin hosted SMS deposits have a variable $\delta^{34}S$ signature in both sulfide and sulfate minerals. Mid-ocean ridge hosted deposits are less-variable. (Data: Anderson et al., 2019; Arnold and Sheppard, 1981; Chiba et al., 1998; de Ronde et al., 2011; Gemmell et al., 2004; Hannington et al., 2005; Herzig et al., 1998a,b; Keith et al., 2016b; Kim et al., 2011; Martin et al., 2020; Styrt et al., 1981; Yeats et al., 2014).

Figure 8: Trace element analysis of pyrite. A) Ratio of trace elements in pyrite at Mala (n=61) to all other Troodos VMS (TO) (Martin et al., 2019, 2020). B) Te vs. Se and C) Co vs. Se for the Mala vs. a 'typical' Troodos deposit – Skouriotissa (Martin et al., 2019). Note varying correlation trends between Mala and Skouriotissa.

Figure 9: Metal sourcing in mafic-hosted VMS deposits. A) The traditional model of metal sourcing in mafic environments (Franklin et al., 2005; Galley et al., 2007). Metal and sulfur are primarily sourced through the leaching of igneous lithologies, epidosite formation and TSR. B) New proposed model for immature mafic VMS deposits, metals are sourced primarily from the contribution of a magmatic volatile phase. The disproportionation of magmatic SO_2 provides the main source of sulfur, TSR the leaching of igneous sulfur and epidosite formation are minor components.

951

Figure 1

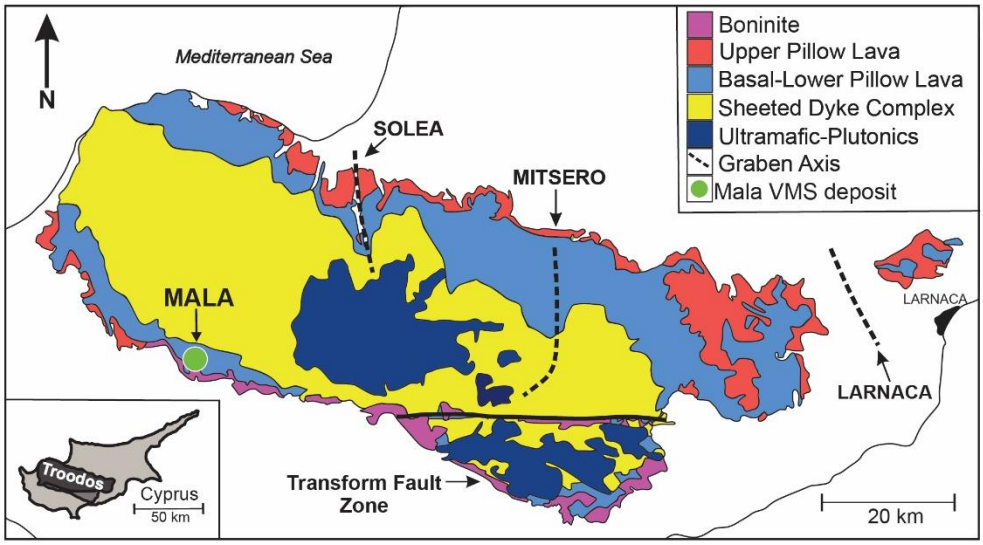
Mediterranean Sea
N
SOLEA
MITSERO
MALA
LARNACA
LARNACA
Boninite
Upper Pillow Lava
Basal-Lower Pillow Lava
Sheeted Dyke Complex
Ultramafic-Plutonics
Graben Axis
Mala VMS deposit
Troodos
Cyprus
50 km
Transform Fault Zone
20 km

952

Figure 2

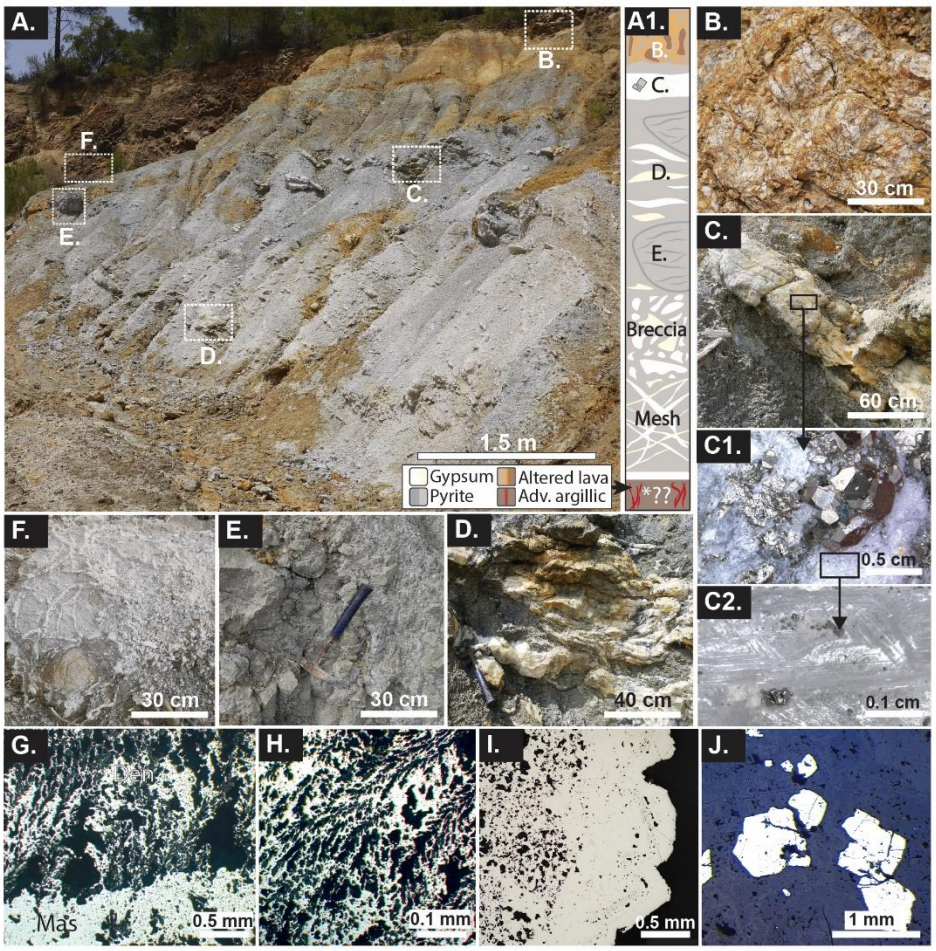
A.
B.
C.
D.
E.
F.
1.5 m
Gypsum
Pyrite
Altered lava
Adv. argillic
A1.
B.
C.
D.
E.
Breccia
Mesh
*??
B.
30 cm
C.
60 cm
C1.
0.5 cm
C2.
0.1 cm
F.
30 cm
E.
30 cm
D.
40 cm
G.
Ves
Mas
0.5 mm
H.
0.1 mm
I.
0.5 mm
J.
1 mm

953

Figure 3

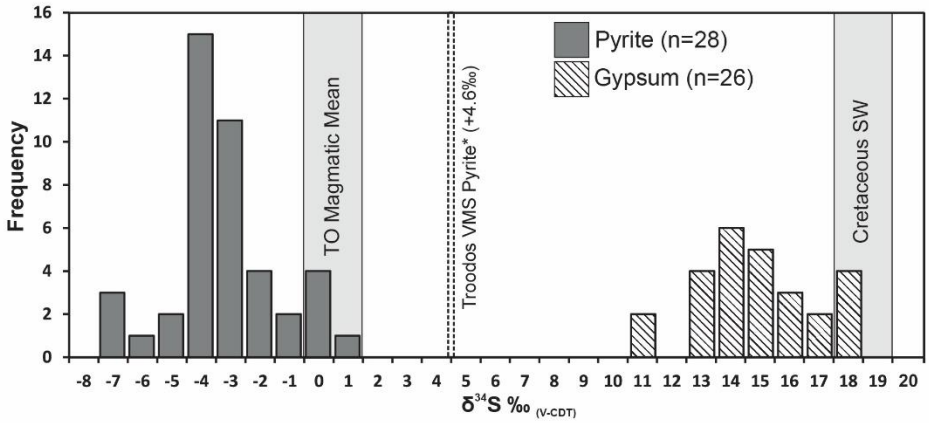
Frequency
16
14
12
10
8
6
4
2
0
-8 -7 -6 -5 -4 -3 -2 -1 0 1 2 3 4 5 6 7 8 9 10 11 12 13 14 15 16 17 18 19 20
δ34S ‰ (V-CDT)
TO Magmatic Mean
Troodos VMS Pyrite* (+4.6‰)
Cretaceous SW
Pyrite (n=28)
Gypsum (n=26)

954

Figure 4

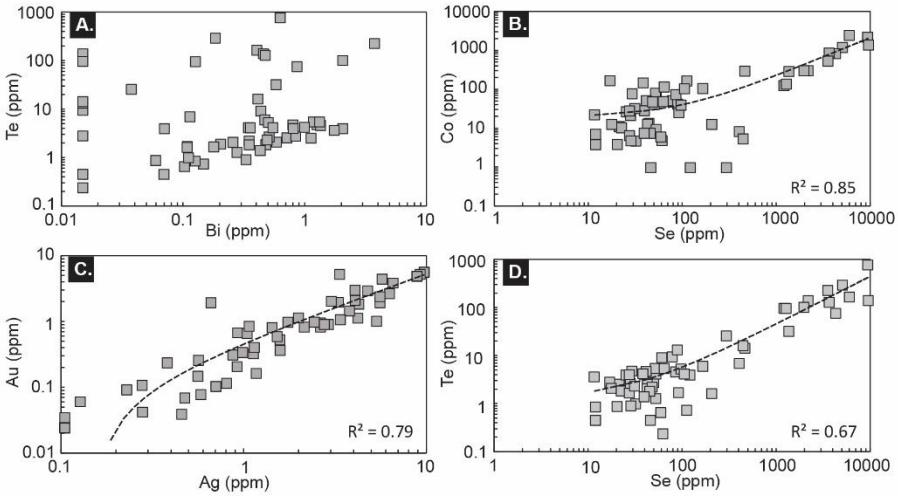
A.
Te (ppm)
Bi (ppm)
B.
Co (ppm)
Se (ppm)
R² = 0.85
C.
Au (ppm)
Ag (ppm)
R² = 0.79
D.
Te (ppm)
Se (ppm)
R² = 0.67

955

Figure 5

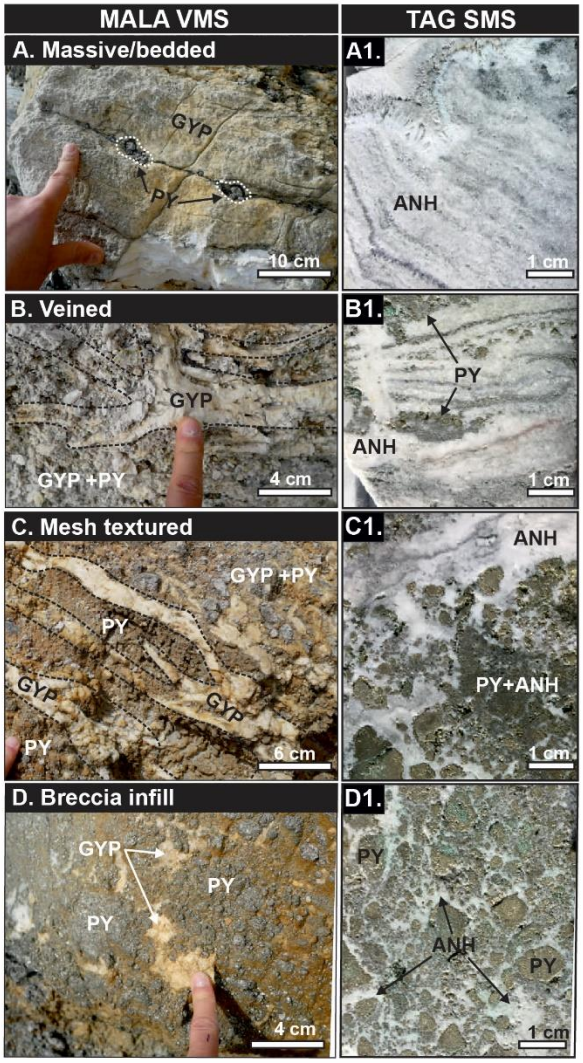
MALA VMS
TAG SMS
A. Massive/bedded
GYP
PY
10 cm
A1.
ANH
1 cm
B. Veined
GYP
GYP +PY
4 cm
B1.
PY
ANH
1 cm
C. Mesh textured
GYP +PY
PY
GYP
GYP
PY
6 cm
C1.
ANH
PY+ANH
1 cm
D. Breccia infill
GYP
PY
PY
4 cm
D1.
PY
ANH
PY
1 cm

956

Figure 6

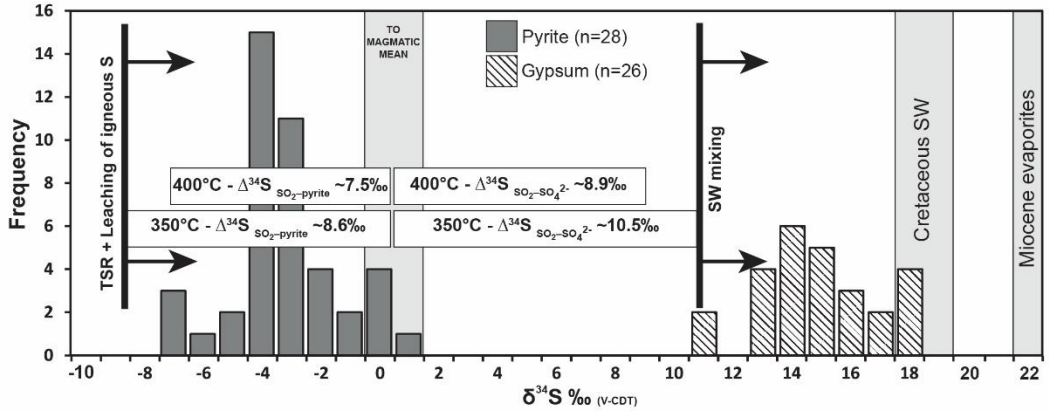
Frequency
δ34S ‰ (V-CDT)
TSR + Leaching of igneous S
TO MAGMATIC MEAN
SW mixing
Pyrite (n=28)
Gypsum (n=26)
400°C - Δ34S SO2–pyrite ~7.5‰
400°C - Δ34S SO2–SO42- ~8.9‰
350°C - Δ34S SO2–pyrite ~8.6‰
350°C - Δ34S SO2–SO42- ~10.5‰
Cretaceous SW
Miocene evaporites

957

Figure 7

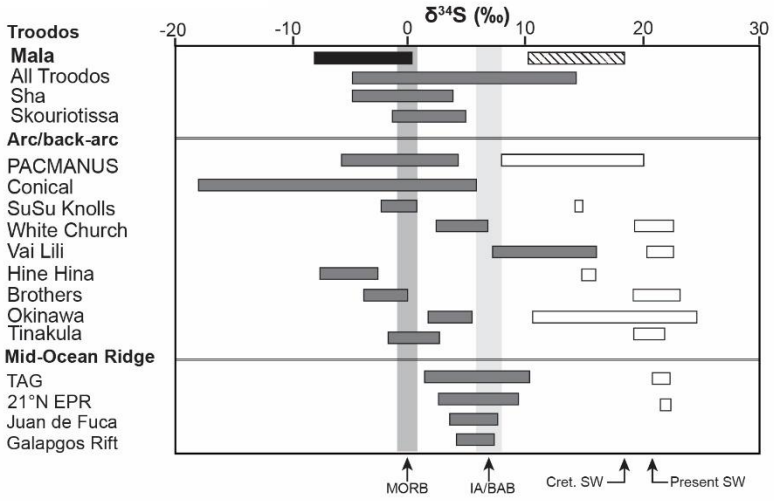
δ34S (‰)
-20
-10
0
10
20
30
Troodos
Mala
All Troodos
Sha
Skouriotissa
Arc/back-arc
PACMANUS
Conical
SuSu Knolls
White Church
Vai Lili
Hine Hina
Brothers
Okinawa
Tinakula
Mid-Ocean Ridge
TAG
21°N EPR
Juan de Fuca
Galapgos Rift
MORB
IA/BAB
Cret. SW
Present SW

958

Figure 8

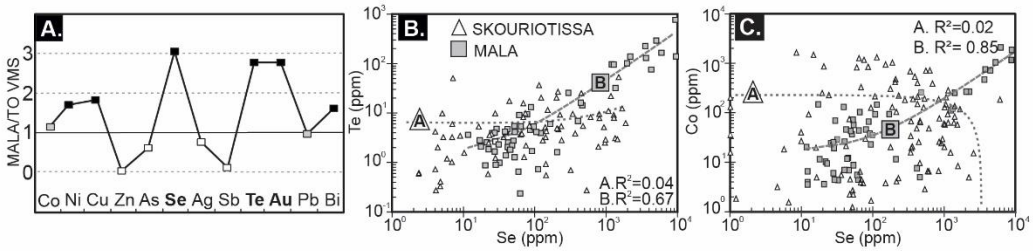
A.
MALA/TO VMS
Co Ni Cu Zn As Se Ag Sb Te Au Pb Bi
B.
SKOURIOTISSA
MALA
Te (ppm)
Se (ppm)
A.R²=0.04
B.R²=0.67
C.
A. R²=0.02
B. R²= 0.85
Co (ppm)
Se (ppm)

959

Figure 9

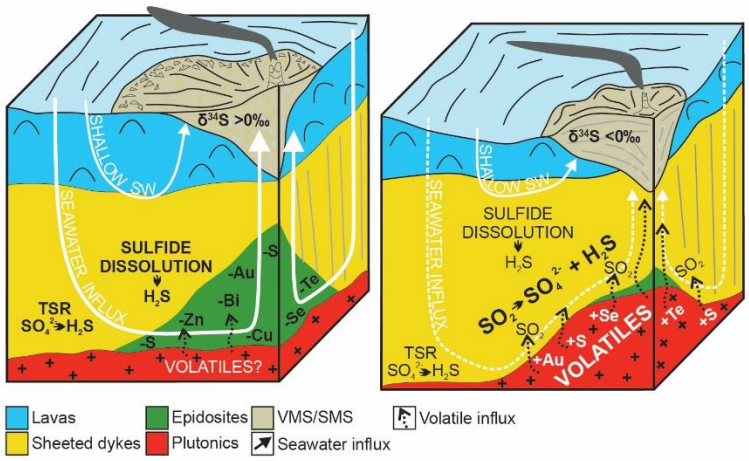
δ34S >0‰
SHALLOW SW
SEAWATER INFLUX
SULFIDE DISSOLUTION
H2S
TSR SO4 2- → H2S
-S
-Au
-Bi
-Zn
-Cu
-Se
-Te
VOLATILES?
δ34S <0‰
SHALLOW SW
SEAWATER INFLUX
SULFIDE DISSOLUTION
H2S
SO4 2- + H2S
SO2
SO2
SO2
+Se
+Te
+S
+Au
VOLATILES
TSR SO4 2- → H2S
Lavas
Sheeted dykes
Epidosites
Plutonics
VMS/SMS
Seawater influx
Volatile influx

960